GALCIT 118 - PROGRESS REPORT NO. 2

Aerojet Contract S-416394-OP

July 1, 1961 - September 30, 1961

FUNDAMENTAL STUDIES RELATING TO THE MECHANICAL BEHAVIOR OF SOLID PROPELLANTS, ROCKET GRAINS AND ROCKET MOTORS

P. J. Blatz

W. L. Ko

A. Zak

October 1961

This program is being supported by the Aerojet-General Corporation, Sacramento Division, under technical cognizance of Dr. F. J. Climent to provide technical support to the Polaris Project

Guggenheim Aeronautical Laboratory

California Institute of Technology

Pasadena, California

TABLE OF CONTENTS *

* The contents of this quarterly progress report comprise only Chapters I and IV. Material for the other chapters will be included in subsequent reports also to be organized as indicated.

I. MECHANICAL BEHAVIOR OF RUBBERY MATERIALS

A. Introduction

In the earlier report the information obtained from both uniaxial and biaxial tension on foam and continuum rubbers was presented. The biaxial data of foam was comparable to the uniaxial data, but it was not so for the continuum rubbers. Namely, the continuum rubbers were found dilating enormously in biaxial tension in which the thickness change was measured by the travelling microscope at the edge of specimens.

Due to the above unusual result, further strip-biaxial tension tests as well as homogeneous - biaxial tension tests were performed, on the same materials SBR --- 500 (1.75 percent S), SBR --- 1500 (3 percent S) and polyurethane foam with an improved technique for measurement of thickness change at the center of the specimens in order to check the dependability of earlier data.

The purpose of this report is to furnish complete set of data to supplement the earlier ones from which the nature of the parameters (W_1, W_2, $dJ_3/d\lambda$, μ , etc.) can be more definitely clarified. Following it the effective Poisson's ratio can be found through which the failure criterion could be established.

B. Experimental Adductions

1. Specimen Geometries

a. Strip-Biaxial Test Specimens:

The working length is again ℓ = 1", the width w was increased nearly twice that of previous test in order to eliminate edge effect, and thickness t for each test are listed on Table I. 1. As before a thin sheet of specimen is glued both sides of both ends on thin metal sheets to prevent lateral contraction. The corners of the plates were rounded to reduce the stress concentration at the corners which cause relatively earlier rupture of the specimen (c.f. Figures 3, 4).

b. Homogeneous - Biaxial Test Specimens:

Square sheets were used. The average size is 3" x 3". The size was varied to meet the different ultimate extension ratios of different materials. Both sides of the four edges and corners of a specimen were glued on hooks at approximately 1/2" interval (c.f. Figures I. 1, I. 5, I. 6). Every hook can easily move along the smooth frame by means of ball bearings attached to it when the specimen is stretched. Thus it will stay perpendicular to the edge of the specimen up to rupture.

2. Test Procedures

All the test specimens were prestressed at constant temperature up to extension ratio of $1.4 \sim 1.5$ once to eliminate hysteresis (hysteresis was nearly zero). In order to read λ_{th} corresponding to the equilibrium state in biaxial and homogeneous-biaxial tension, the cross head of INSTRON machine was stopped and the chart was allowed to continue on until the load-time curve leveled off. Instead of measuring λ_{th} at the edge of the specimen in biaxial tension by travelling microscope (this method was used in the previous test), λ_{th} was measured at the center of a specimen by micrometers for both types of biaxial tension (c.f. Figures I. 1, I. 2).

The micrometers used could measure thickness up to 10^{-4} in. accuracy.

Again from the test date the following curves were plotted (c.f. Figures I. 7 - I. 31):

a. Strip-Biaxial Tension:

i) σ_{bi} vs λ

ii) $\lambda\sigma_{bi}$ vs $\lambda^2 - \lambda^2_{th}$

Since $J_3 = \lambda\lambda_{th} \approx 1$, the equation $\frac{\lambda\sigma_{bi}}{\lambda^2-\lambda^2_{th}} = 2W_1 + \frac{2W_2}{\lambda^2\lambda^2_{th}}$ is reduced to $\lambda\sigma_{bi} \approx 2(W_1+W_2)(\lambda^2-\lambda^2_{th})$. Thus in this test W_1 and W_2 cannot be found separately.

iii) λ_{th} vs λ

iv) $J_3 (\approx \lambda\lambda_{th})$ vs λ

b. Homogeneous-Biaxial Tension:

i) σ_{h-b} vs λ

ii) $\frac{\lambda\sigma_{h-b}}{\lambda^2-\lambda_{th}^2}$ vs $\frac{1}{\lambda^2\lambda_{th}^2}$

iii) λ_{th} vs λ

iv) $J_3 (= \lambda^2\lambda_{th})$ vs λ

3. Results and Discussion

A set of derived information obtained from Figures I. 7 - I. 31 is shown in Table I. 1. The following items were noted in the present tests.

i) For foam rubber the measurement of λ_{th} at the edge and at the specimen center gives similar data as before.

ii) The continuum rubbers do not dilate. Since λ_{th} at edge is greater than that at the center and this edge effect dies out at 1" from the edge (c.f. Figure I. 11).

iii) For foam rubber W_1 and W_2 are both positive constant in biaxial tension, but W_1 is negative in homogeneous-biaxial tension. On average, $W_1 = 0$, $W_2 > 0$. The shear modulus μ stays almost the same value in both types of biaxial-tension. But it is less than that in uniaxial tension. (i.e. $\left\{\begin{matrix}\mu_{bi} \\ \mu_{h-b}\end{matrix}\right\} = 0.86\,\mu_{uni}$)

iv) For continuum rubbers, $W_2 = 0$, $\mu_{h-b} \approx \mu_{uni}$ in homogeneous-biaxial tension. In biaxial tension $\mu_{bi} \approx 0.74\,\mu_{uni}$.

v) $W_3 = 0$ for continuum rubbers and $W_3 > 0$ for foam.

Under the assumption that W_1 and W_2 are constant; $W_1 = \frac{\mu}{2} f$, $W_2 = \frac{\mu}{2}(1-f)$, $W_3 = W_3(J_3)$.

For uniaxial tensions in lateral direction Equation I. 23 of Progress Report No. 1 becomes

$$\frac{W_3}{\mu_{uni}} = -\left[\frac{f}{\lambda} - \frac{(1-f)\lambda}{J_3^2}\right] , \qquad J_3 = \lambda\lambda_{lat}^2 \tag{I. 1}$$

and λ can be expressed in term of J_3 from J_3 vs λ curve.

Similarly for biaxial tension

$$\frac{W_3}{\mu_{bi}} = -\left[f\frac{J_3}{\lambda^2} - \frac{(1-f)\lambda^2}{J_3^3}\right] , \qquad J_3 = \lambda\lambda_{th} \tag{I. 2}$$

and for homogeneous-biaxial tension

$$\frac{W_3}{\mu_{h-b}} = -\left[\frac{f J_3}{\lambda^4} - \frac{(1-f)\lambda^4}{J_3^3}\right] , \qquad J_3 = \lambda^2\lambda_{th} \tag{I. 3}$$

For <u>continuum rubbers:</u>

$W_1 = \frac{\mu}{2}$, $W_2 = 0$ so W can be expressed as:

$$W = \frac{\mu}{2}(J_1 - 3) + F(J_3) \tag{I. 4}$$

and from comparison with linear theory the leading terms becomes

$$W = \frac{\mu}{2}(J_1 - 3) - \mu(J_3 - 1) + \left(K + \frac{\mu}{3}\right)\frac{(J_3-1)^2}{2} + \cdots \tag{I. 5}$$

Then the distortion and dilation strain energy function could be written in the form

$$W_{dist.} \equiv \frac{\mu}{2}(J_1 - 3) - \mu(J_3 - 1) + \frac{\mu}{3}\frac{(J_3-1)^2}{2} \tag{I. 6}$$

$$W_{dil.} \equiv K \frac{(J_3-1)^2}{2} \tag{I. 7}$$

For <u>foam rubber:</u>

$W_1 = 0$, $W_2 = \frac{\mu}{2}$ and W is of the form

$$W = \frac{\mu}{2}(J_2-3) + G(J_3) \tag{I. 8}$$

from comparison with linear theory the leading terms becomes

$$W = \frac{\mu}{2}(J_2-3) + \mu(J_3-1) + (K-\frac{5}{3}\mu)\frac{(J_3^2-1)}{2} + \cdots \tag{I. 9}$$

or $$W = \frac{\mu}{2}(J_2-3) + \mu \ln J_3 + (K-\frac{2}{3}\mu)\frac{(J_3^2-1)}{2} + \cdots \tag{I. 10}$$

and $$W_3 = \frac{\mu}{J_3} + (K-\frac{2}{3}\mu)(J_3-1) + \cdots \tag{I. 11}$$

now we want to compare this with the experimental result.

From equations (I. 1), (I. 2) and I. 3) we have

$$W_{3\,uni} = \frac{\mu\lambda}{J_3^2} = \frac{\mu}{\alpha J_3} \quad , \quad \alpha = \frac{dJ_3}{d\lambda} = \frac{J_3}{\lambda} \tag{I. 12}$$

$$W_{3\,bi} = \frac{\mu\lambda^2}{J_3^3} = \frac{\mu}{\beta^2 J_3} \quad , \quad \beta = \frac{dJ_3}{d\lambda} = \frac{J_3}{\lambda} \tag{I. 13}$$

$$W_{3\,h\text{-}b} = \frac{\mu\lambda^4}{J_3^3} = \frac{\mu J_3}{\gamma^4} \quad , \qquad \gamma = \frac{dJ_3}{d\lambda} = \frac{J_3}{\lambda} \tag{I. 14}$$

From data we find

$$\frac{1}{\alpha} = \frac{1}{0.455} = 2.2 \quad , \quad \frac{1}{\beta^2} = \frac{1}{(0.615)^2} = 2.64 \, , \quad \frac{1}{\gamma^4} = \frac{1}{(1.43)^4} = 0.24 \tag{I. 15}$$

$$\frac{1}{\alpha} : \frac{1}{\beta^2} : \frac{1}{\gamma^4} \approx 1 : 1.2 : 0.1 \rightsquigarrow 1 : 1 : 0.1 \tag{I. 16}$$

Actually we may consider $\alpha \approx \beta^2$ then W_3 has two types of experimental forms:

$$W_3 = \frac{\mu}{\alpha J_3} \tag{I. 17}$$

$$W_3 = \frac{\mu J_3}{10\alpha} \tag{I. 18}$$

From equations (I. 9), (I. 10), (I. 17) and (I. 18) we will investigate more fully a better expression of W later.

TABLE I. LIST OF EXPERIMENTAL RESULTS

BIAXIAL TENSION				
MATERIALS	SBR-1500 (1.75% S)	SBR-1500 (3% S)	PU-FOAM (47% VOID)	
SAMPLE DIMENSIONS $\ell \times w \times t$ $\ell : w : t$	$64/64 \quad 744/64 \times 5/64$ 12.8 : 148.8 : 1	$64/64 \times 744/64 \times 5/64$ 12.8 : 148.8 : 1	$8/8 \times 48/8 \times 3/8$ 2.7 : 16 : 1	
AMBIENT TEMPERATURE °F	75 72	73 75	75 75	
σ^*_{bi}, psi.	90.1 85.9	100.5 103.4	19.2 22.3	
λ^*	1.90 1.90	1.60 1.70	1.80 2.00	
λ^*_{th}	0.531 0.542	0.595 0.580	0.824 0.781	
$J_3^* (= \lambda \lambda_{th})$	1.009 1.030	0.951 0.986	1.48 1.56	
W^*, $\frac{\text{in-lbs}}{\text{in}^3}$	57 55	57 67	17.3 12.2	
$2(W_1+W_2) = \mu$, psi.	56 53	75 73	27 $\{W_1 = 2, W_2 = 11.5$ 29 $\{W_1 = 2, W_2 = 12.5$	
$dJ_3/d\lambda$	0 0	0 0	0.62 0.62	

HOMOGENEOUS-BIAXIAL TENSION				
MATERIALS	SBR-1500 (1.75% S)	SBR-1500 (3% S)	PU-FOAM (47% VOID)	
SAMPLE DIMENSIONS $\ell \times w \times t$ $\ell : w : t$	$192/64 \times 192/64 \times 5/64$ 38.4 : 38.4 : 1	$192/64 \times 192/64 \times 5/64$ 38.4 : 38.4 : 1	$22/8 \times 22/8 \times 3/8$ 7.3 : 7.3 : 1	
AMBIENT TEMPERATURE °F	75 73	75 76	73 73	
$\sigma^*_{h\text{-}b}$, psi.	91.4 94.7	94.9 68.0	20.8 20.6	
λ^*	1.39 1.41	1.4 1.2	1.53 1.58	
λ^*_{th}	0.518 0.511	0.559 0.731	0.765 0.750	
$J_3^* (= \lambda^2 \lambda_{th})$	0.985 1.008	1.052 1.077	1.782 1.865	
W^*, $\frac{\text{in-lbs}}{\text{in}^3}$	23 24	22 11	8 9	
W_1, psi.	78 78	87 87	−2.5 −2.5	
W_2, psi.	0 0	0 0	16.5 15.5	
μ, psi.	78 78	87 87	28 26	
$dJ_3/d\lambda$	0 0	0 0	1.43 1.41	

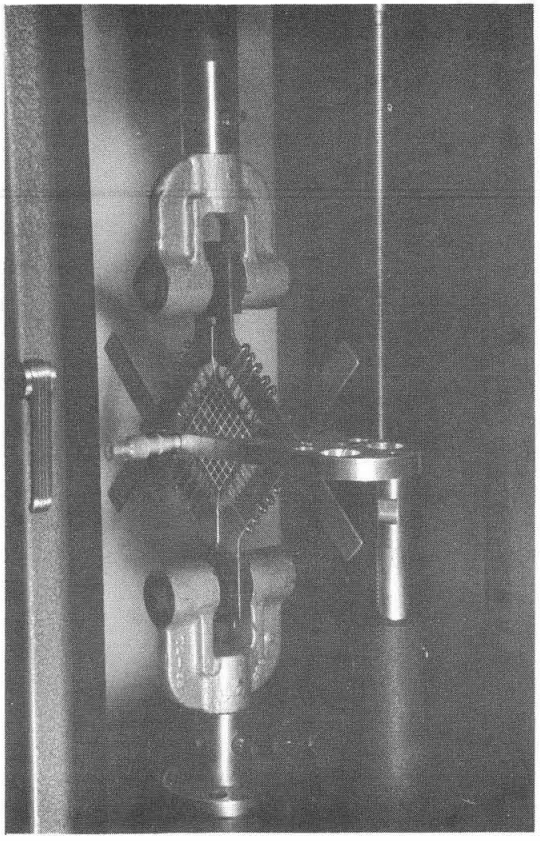

Fig. I.1. Homogeneous-Biaxial Tension

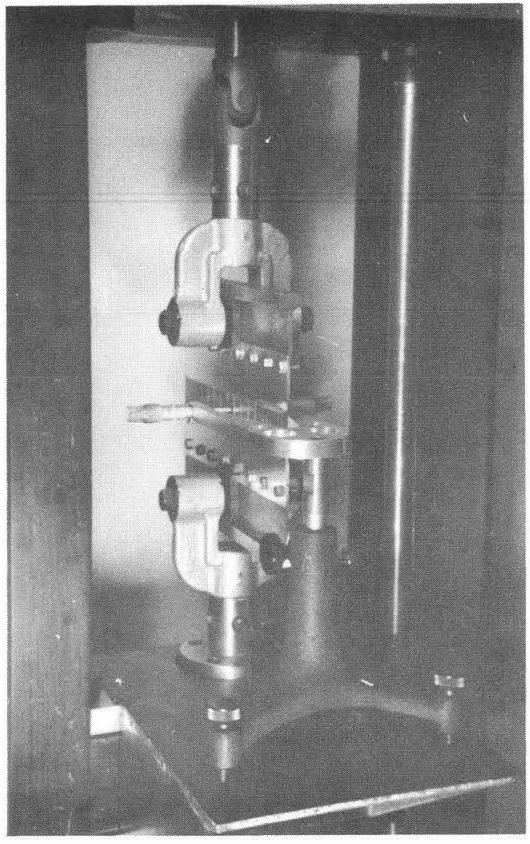

Fig. I.2. Strip-Biaxial Tension

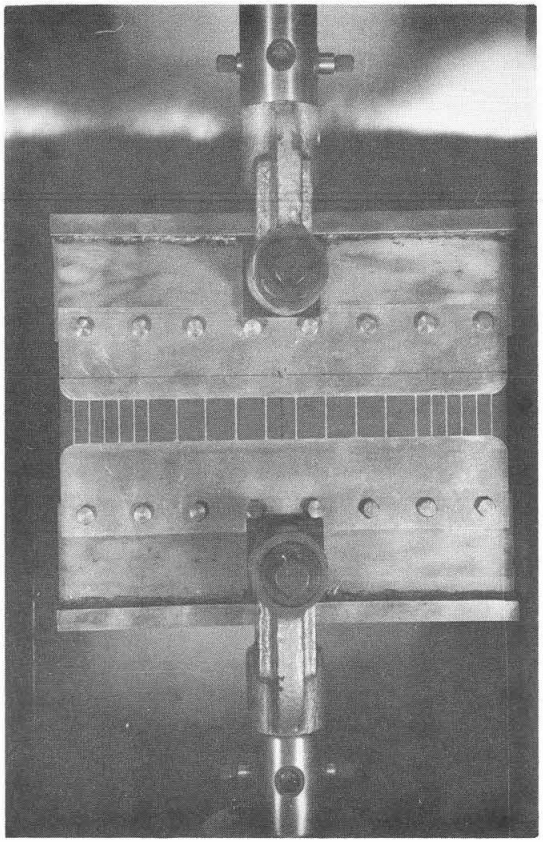

Fig. I.3. Strip-Biaxial Tension at $\lambda = 1$

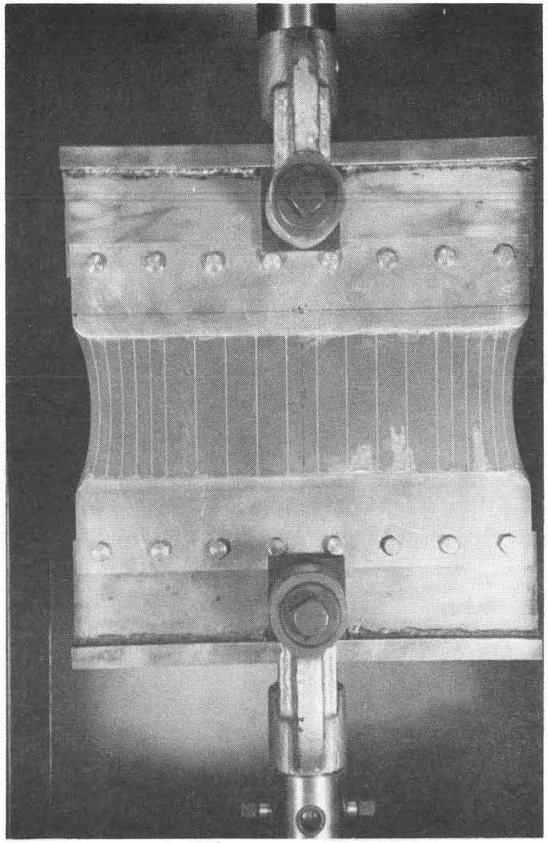

Fig. I.4. Strip-Biaxial Tension at $\lambda = 3.5$

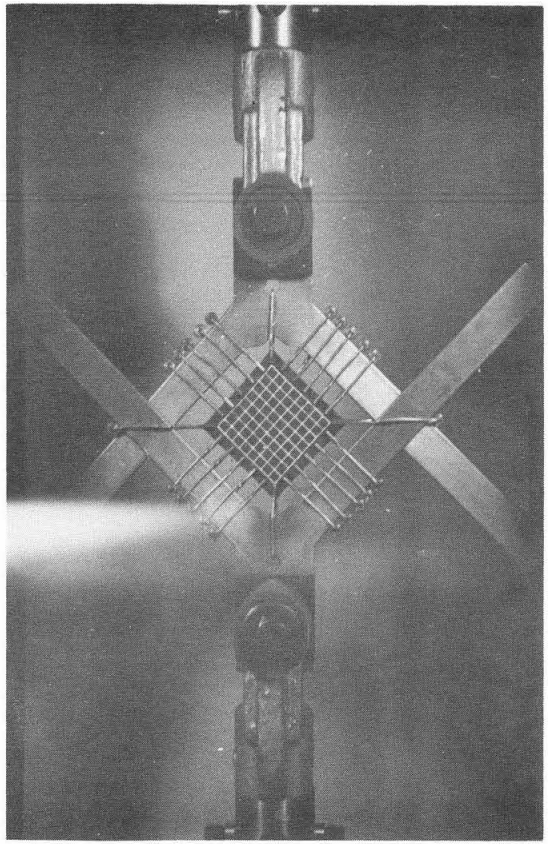

Fig. I.5. Homogeneous-Biaxial Tension at $\lambda = 1$

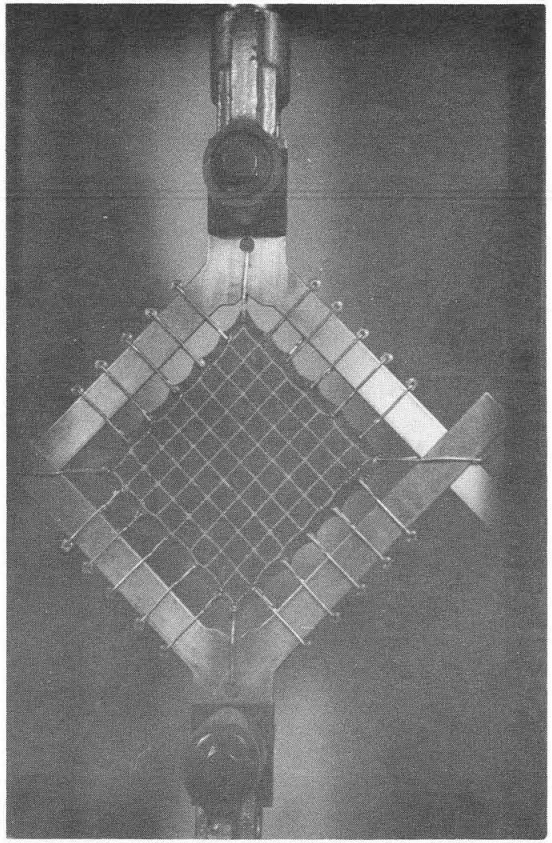

Fig. I.6. Homogeneous-Biaxial Tension at $\lambda = 2.33$

FIG. I.7. BIAXIAL STRESS VS. LONGITUDINAL EXTENSION RATIO

SBR-1500 (1.75% S)

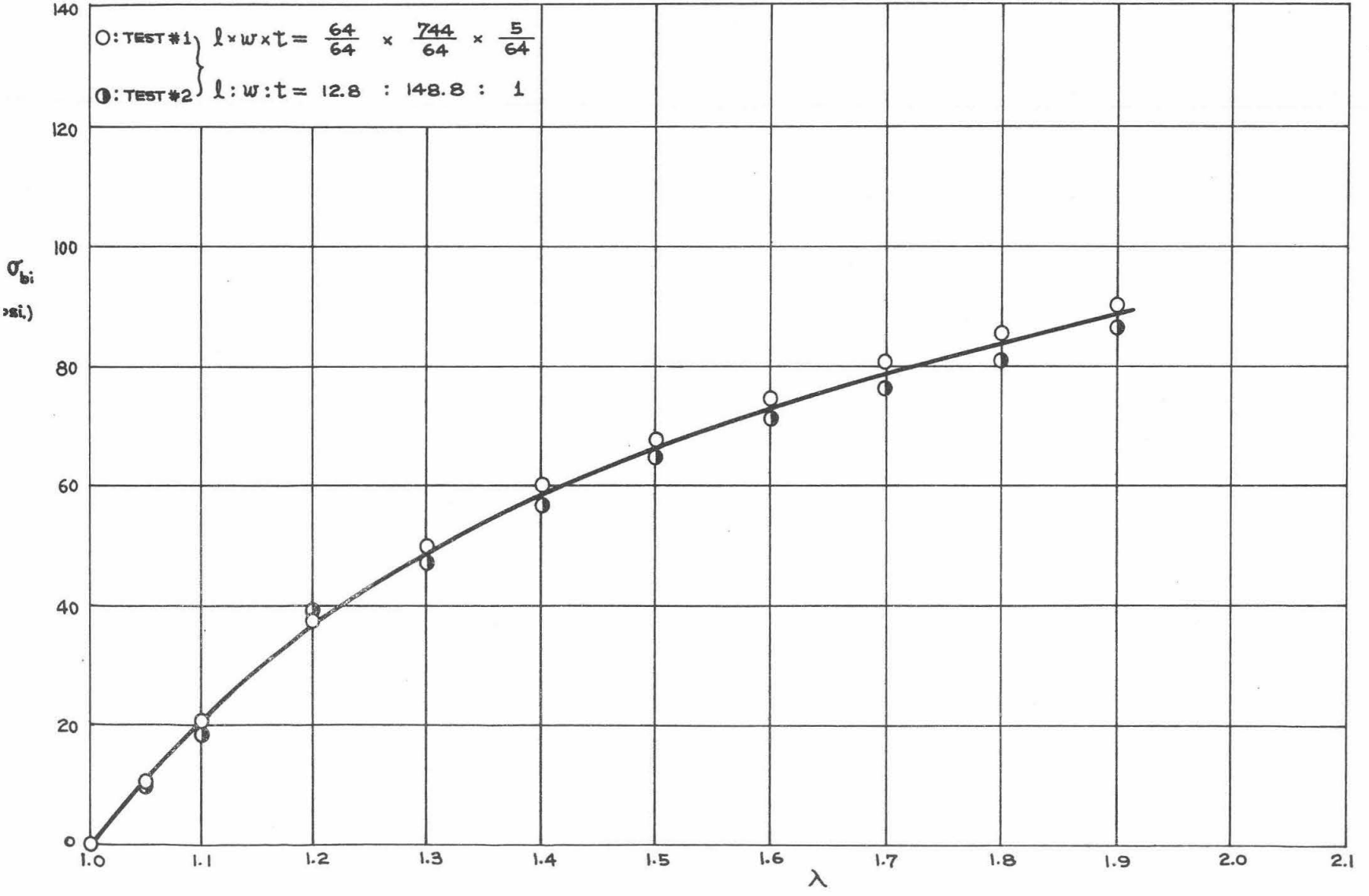

FIG. I. 8. EVALUATION OF $W_1 + W_2$ FROM RECTIFIED BIAXIAL DATA

SBR-1500 (1.75% S)

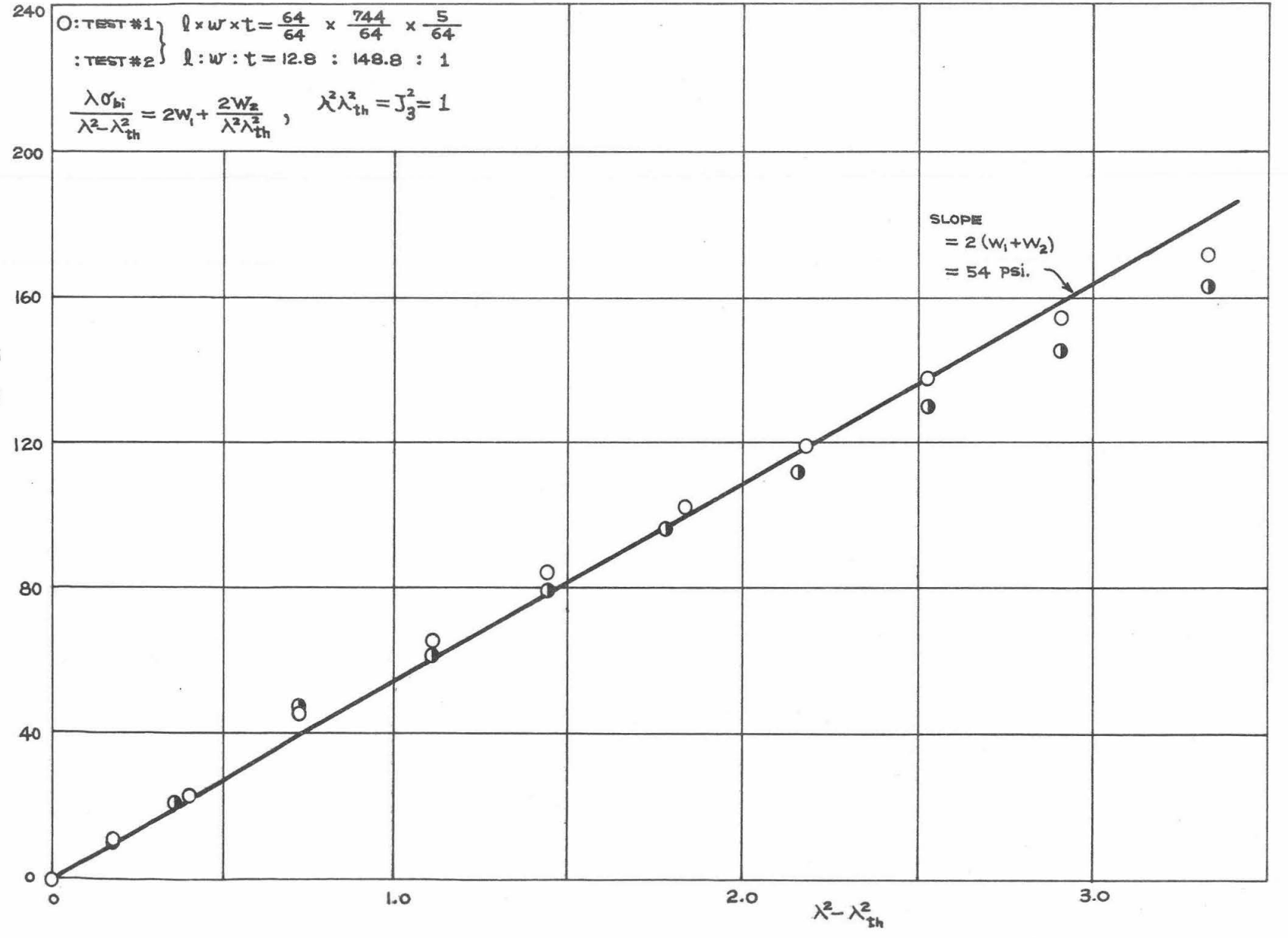

FIG. I. 9. BIAXIAL THICKNESS CONTRACTION RATIO VS. LONGITUDINAL EXTENSION RATIO

SBR-1500 (1.75% S)

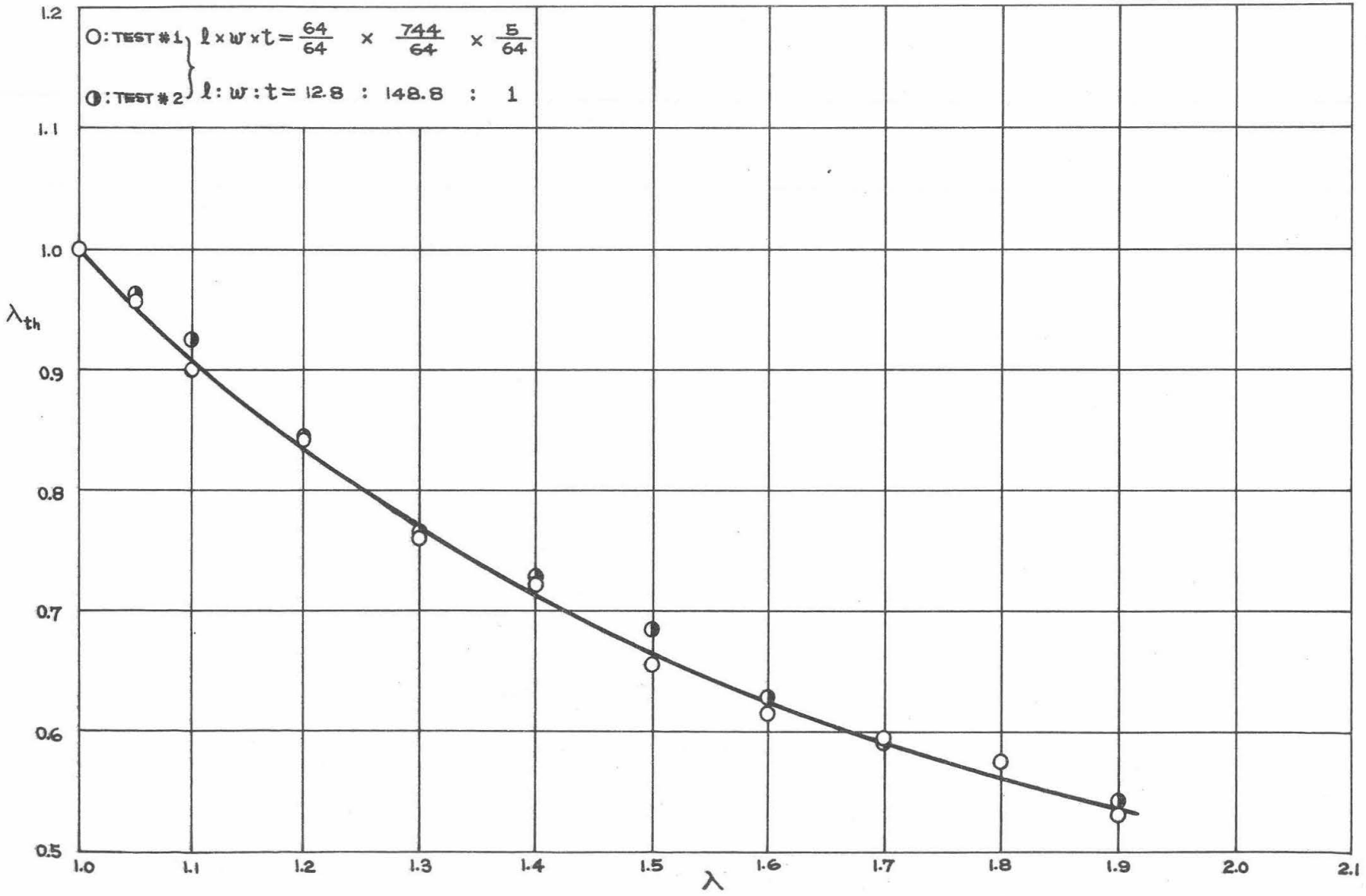

FIG. I. 10. BIAXIAL DILATATION VS. LONGITUDINAL EXTENSION RATIO

SBR-1500 (1.75% S)

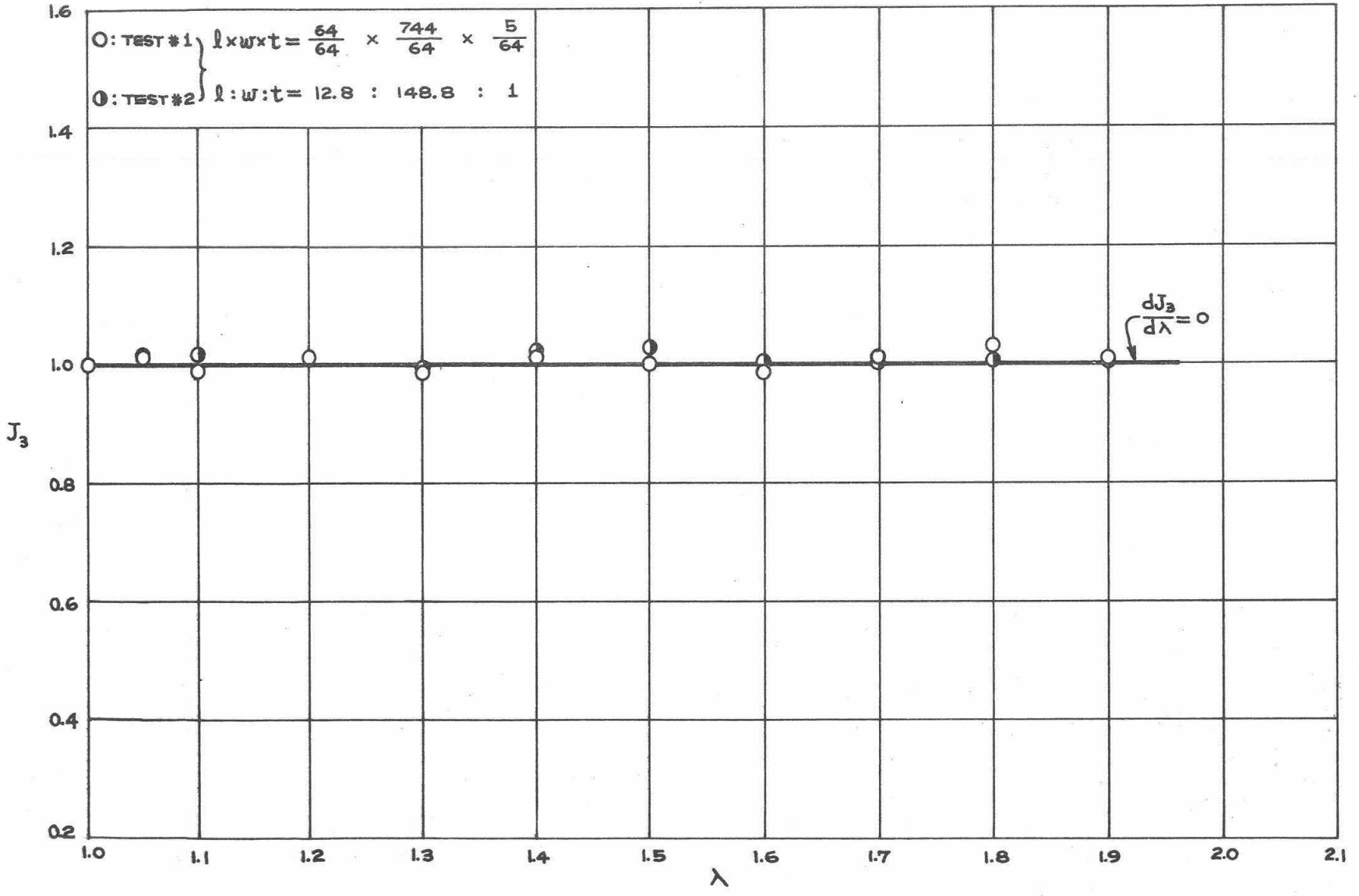

FIG. I.11. CHANGE IN λ_{th} ACROSS WIDTH OF BIAXIAL SPECIMEN AT $\lambda = 1.8$ ($\lambda_{ult} = 1.9$)
SBR-1500 (1.75% S)

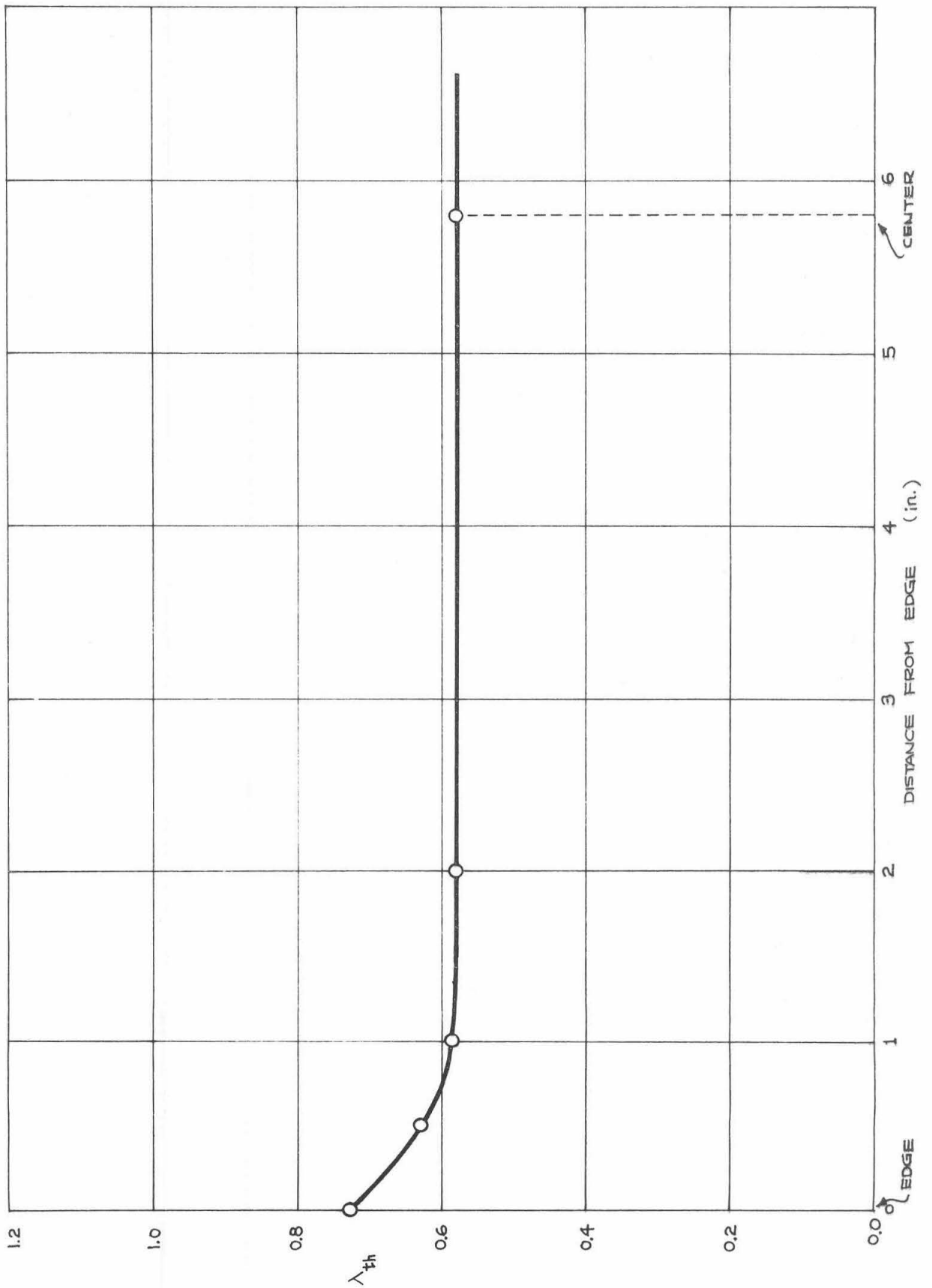

FIG. I.12. HOMOGENEOUS-BIAXIAL STRESS VS. LONGITUDINAL EXTENSION RATIO

SBR-1500 (1.75% S)

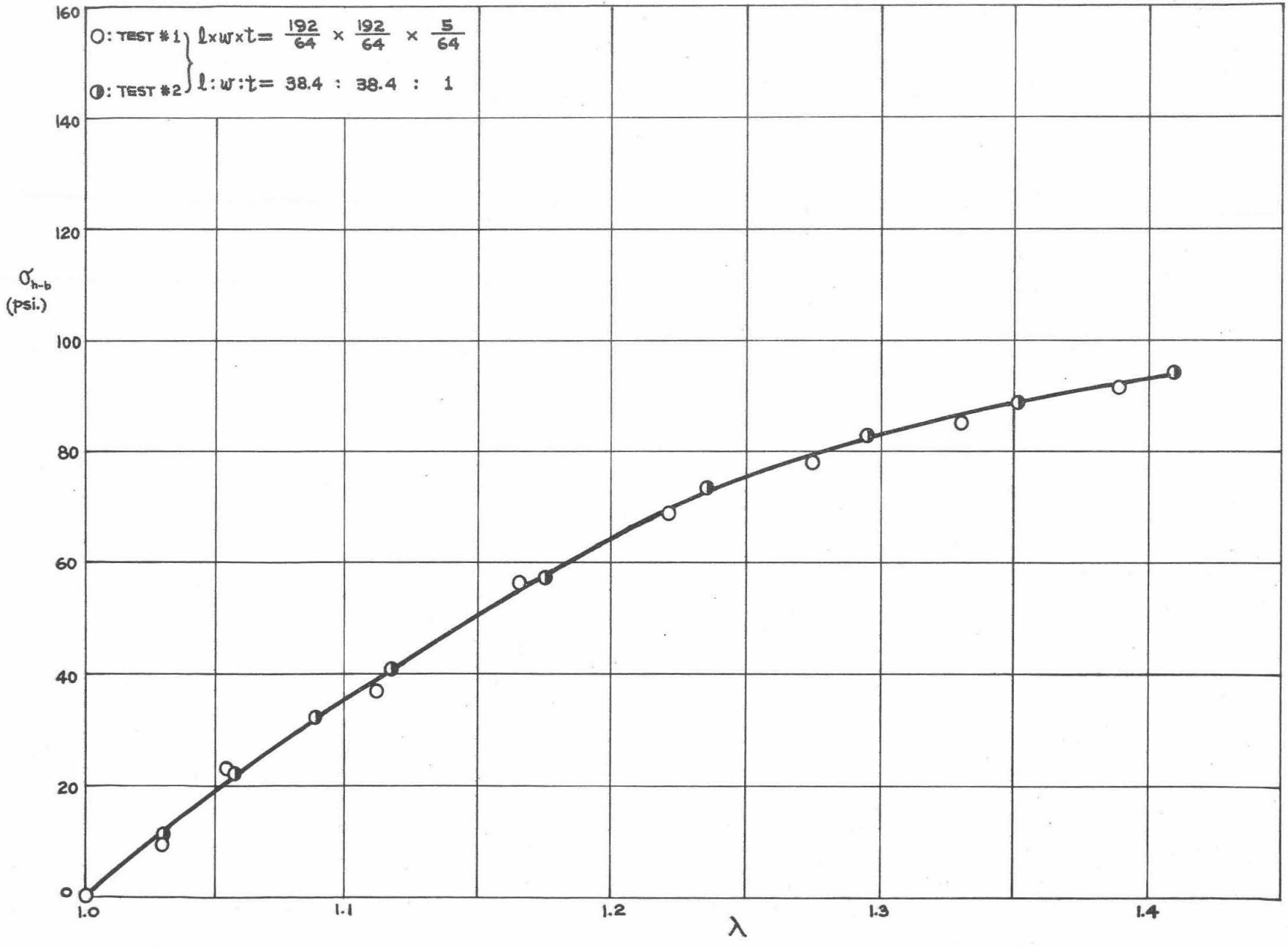

FIG. I.13. EVALUATION OF W_1 & W_2 FROM RECTIFIED HOMOGENEOUS-BIAXIAL DATA

SBR-1500 (1.75% S)

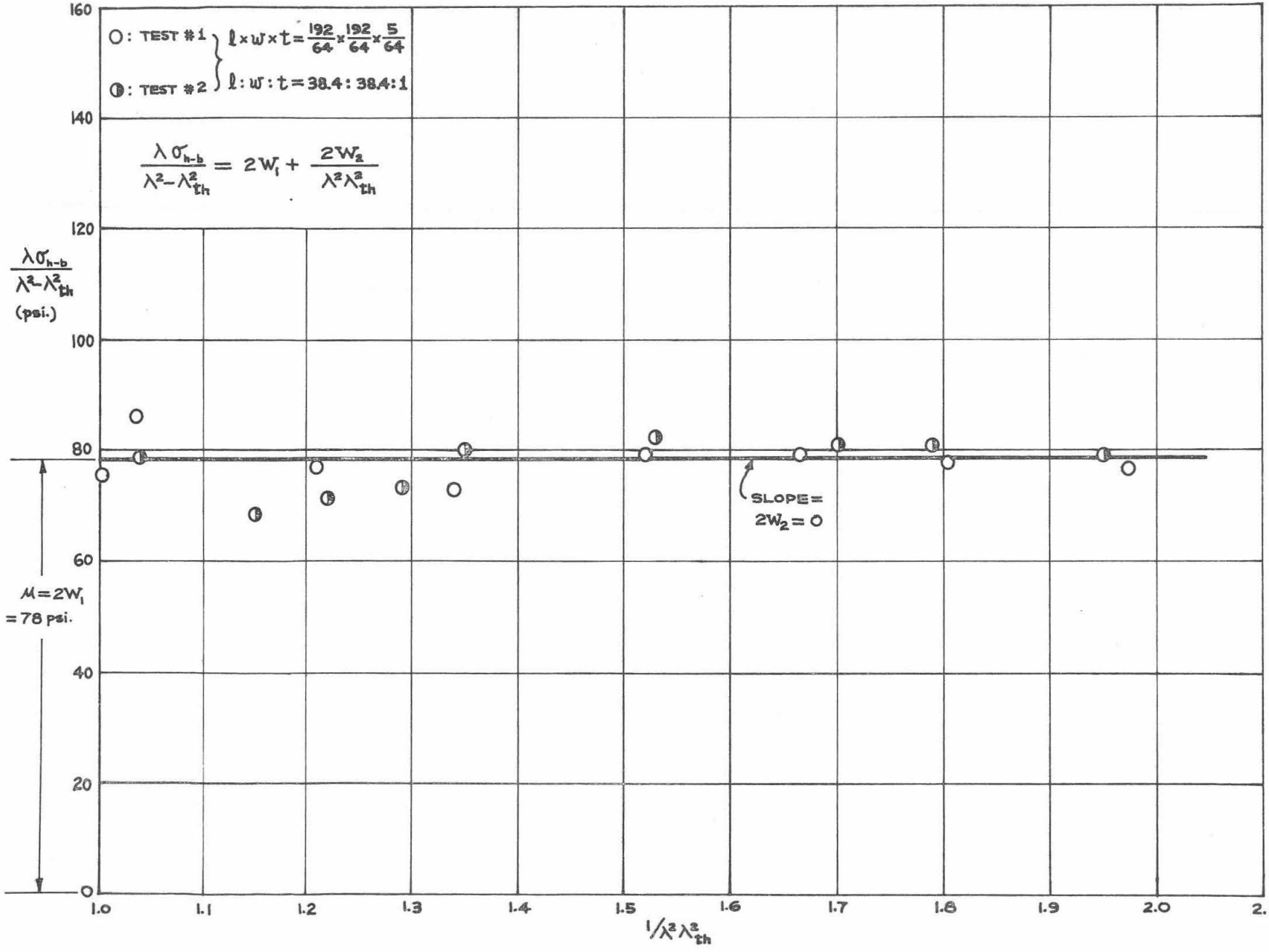

FIG.I.14. HOMOGENEOUS-BIAXIAL THICKNESS CONTRACTION RATIO VS. LONGITUDINAL EXTENSION RATIO

SBR-1500 (1.75% S)

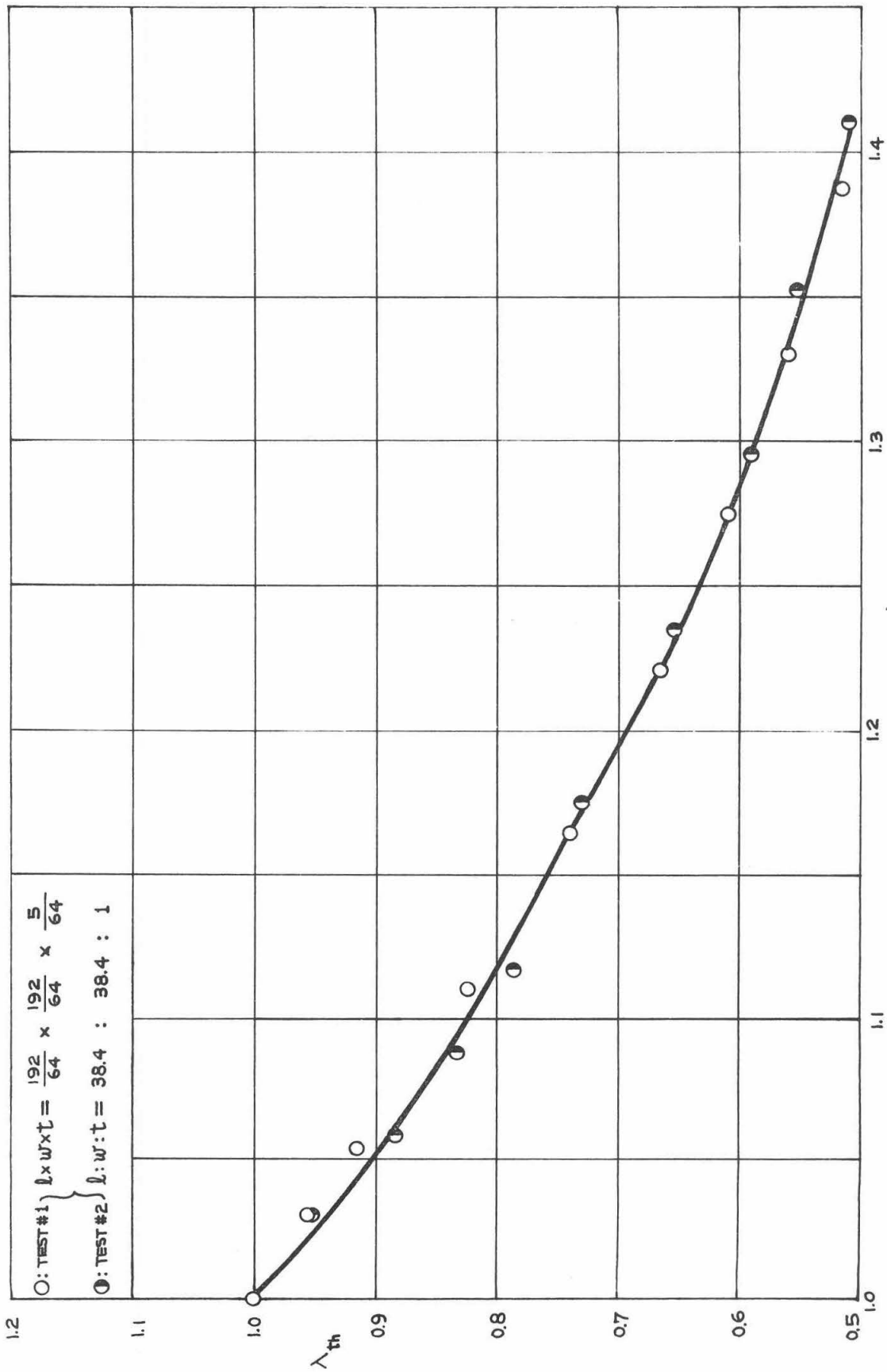

FIG. I.15. HOMOGENEOUS - BIAXIAL DILATATION VS. LONGITUDINAL EXTENSION RATIO

SBR-1500 (1.75 % S)

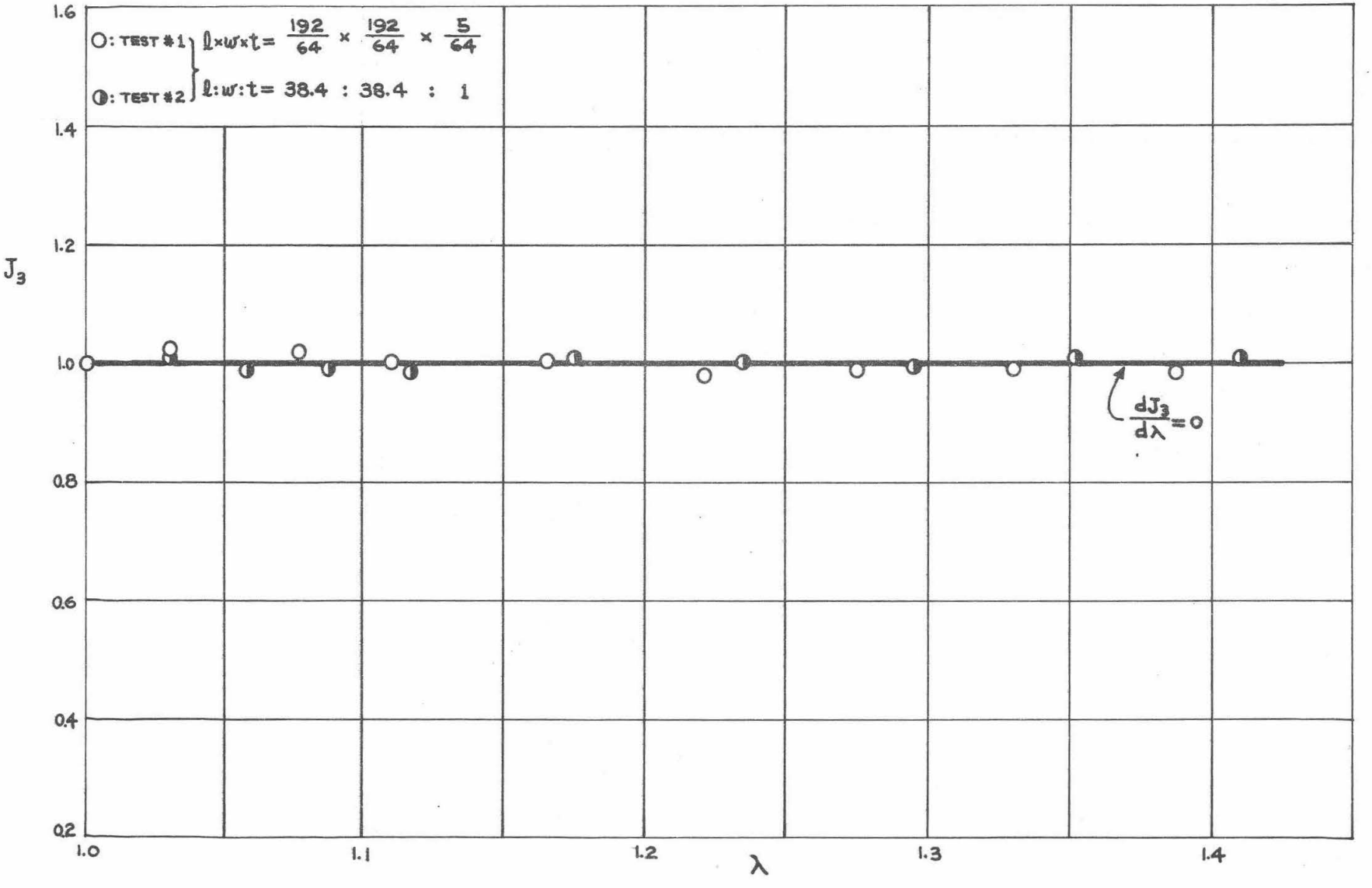

FIG. I.16. BIAXIAL STRESS VS. LONGITUDINAL EXTENSION RATIO

SBR-1500 (3% S)

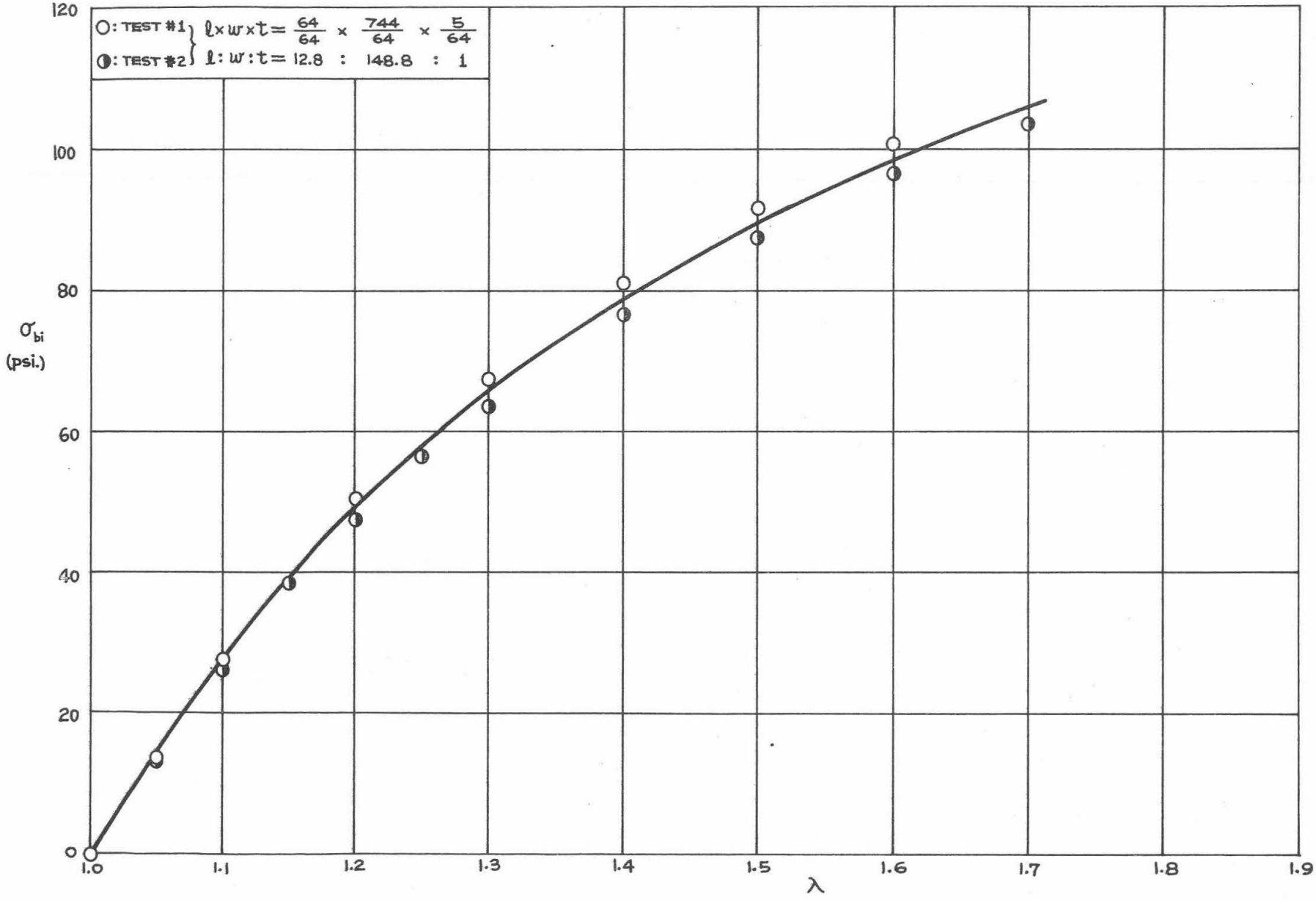

FIG. I.17. EVALUATION OF $W_1 + W_2$ FROM RECTIFIED BIAXIAL DATA

SBR-1500 (3 % S)

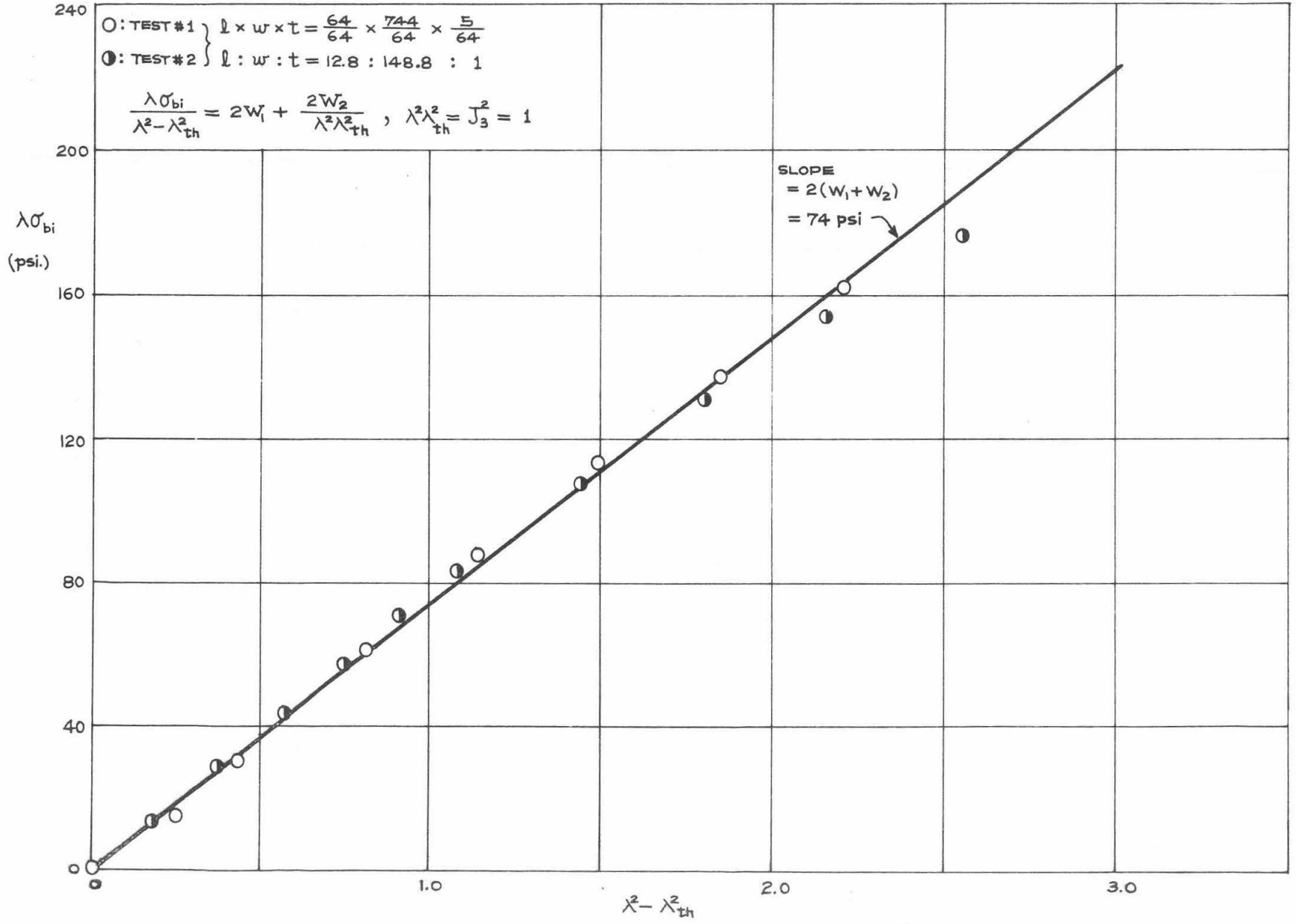

FIG.I.18. BIAXIAL THICKNESS CONTRACTION RATIO VS. LONGITUDINAL EXTENSION RATIO

SBR-1500 (3% S)

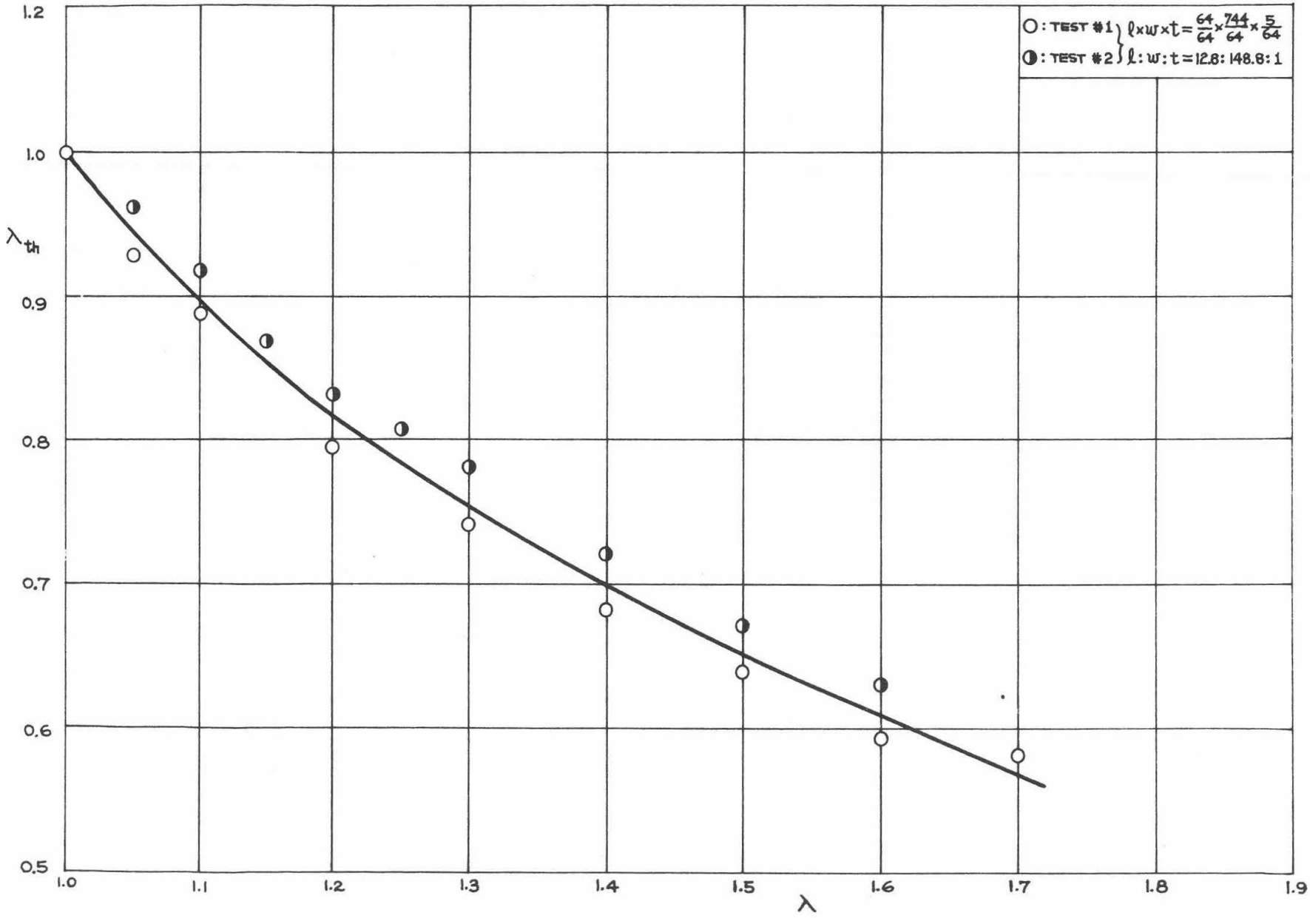

FIG. I.19. BIAXIAL DILATATION VS. LONGITUDINAL EXTENSION RATIO

SBR-1500 (3% S)

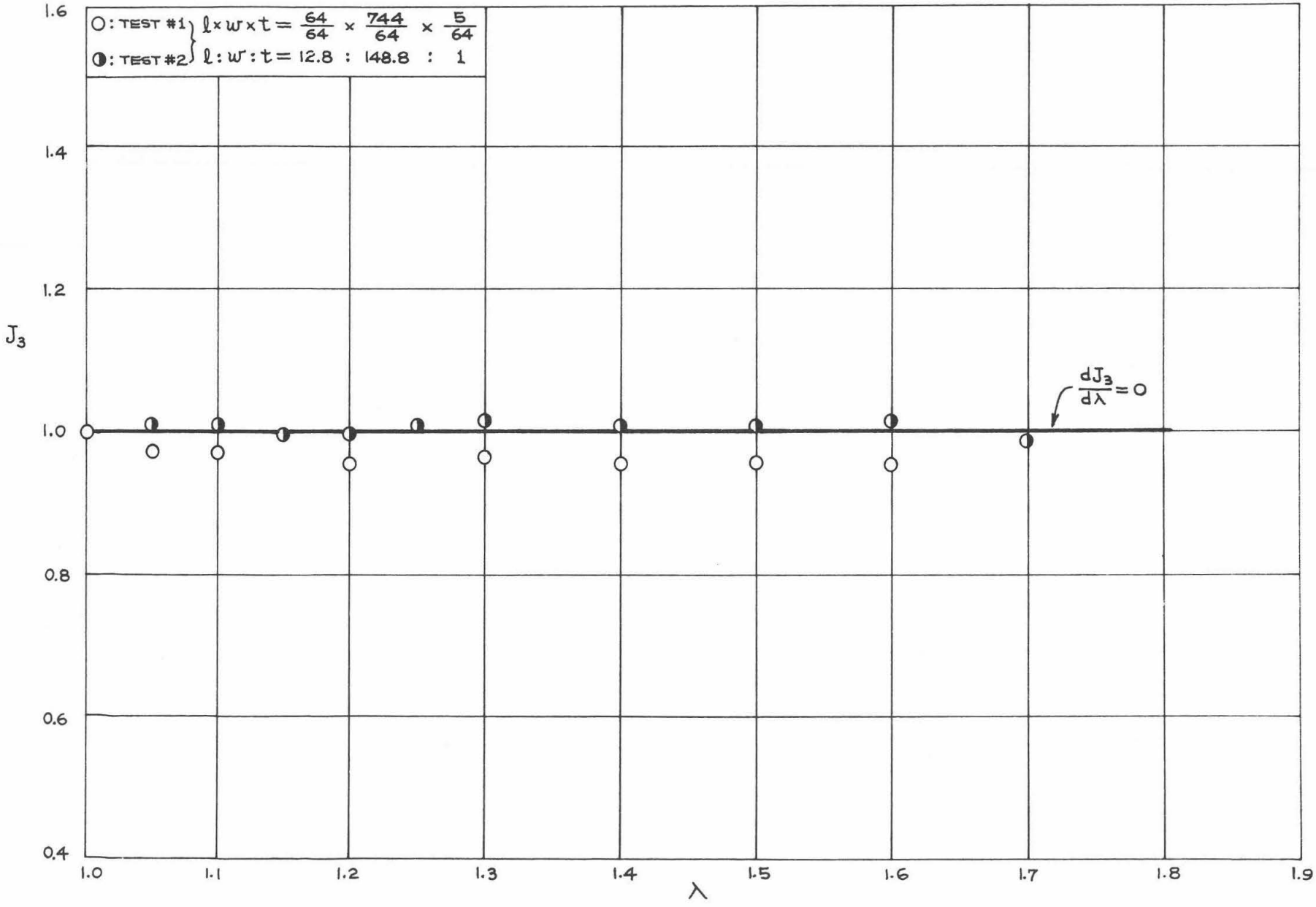

FIG. I. 20. HOMOGENEOUS–BIAXIAL DILATATION VS. LONGITUDINAL EXTENSION RATIO

SBR-1500 (3 % S)

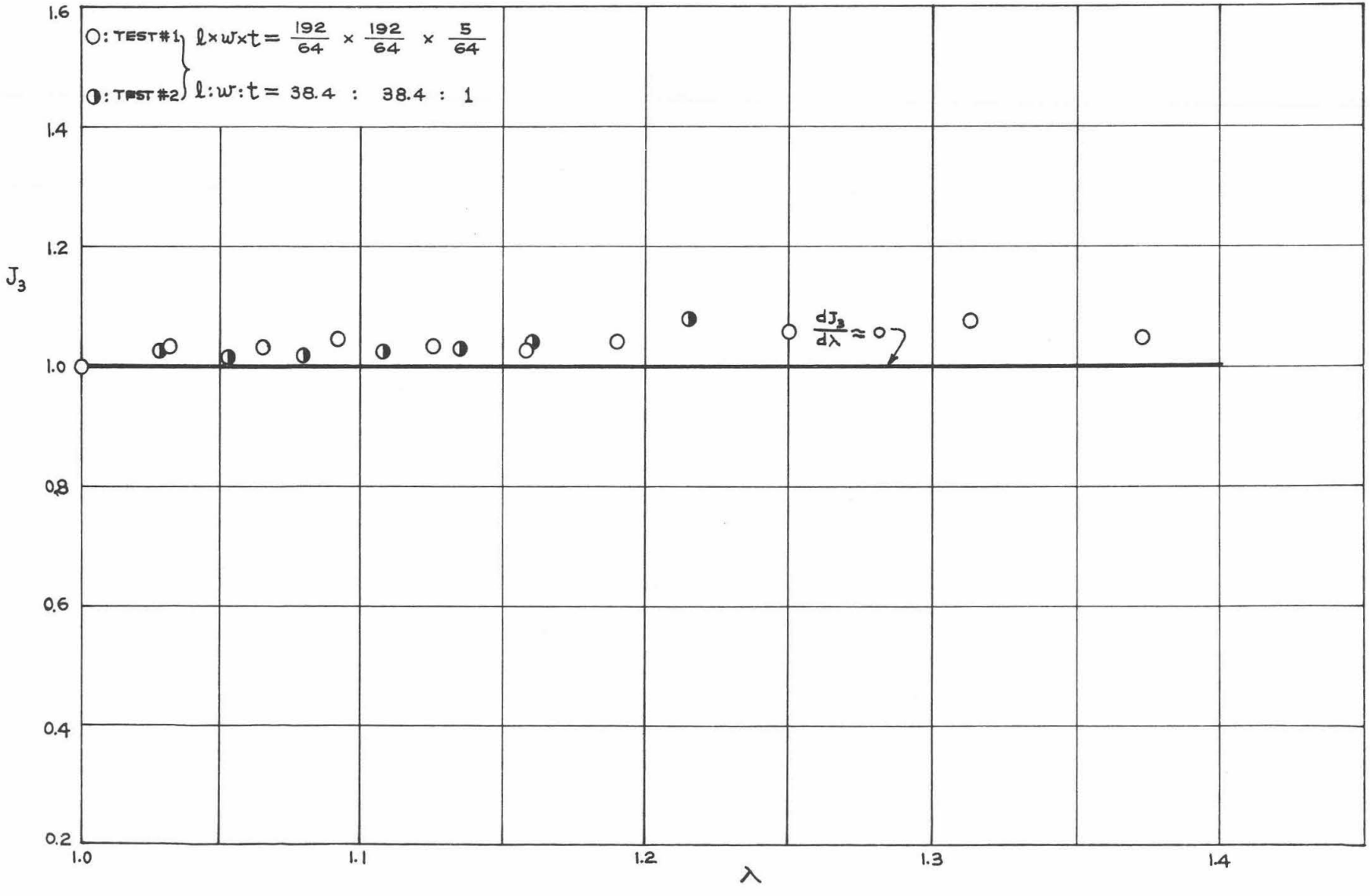

FIG.I.21. HOMOGENEOUS-BIAXIAL STRESS VS. LONGITUDINAL EXTENSION RATIO

SBR-1500 (3% S)

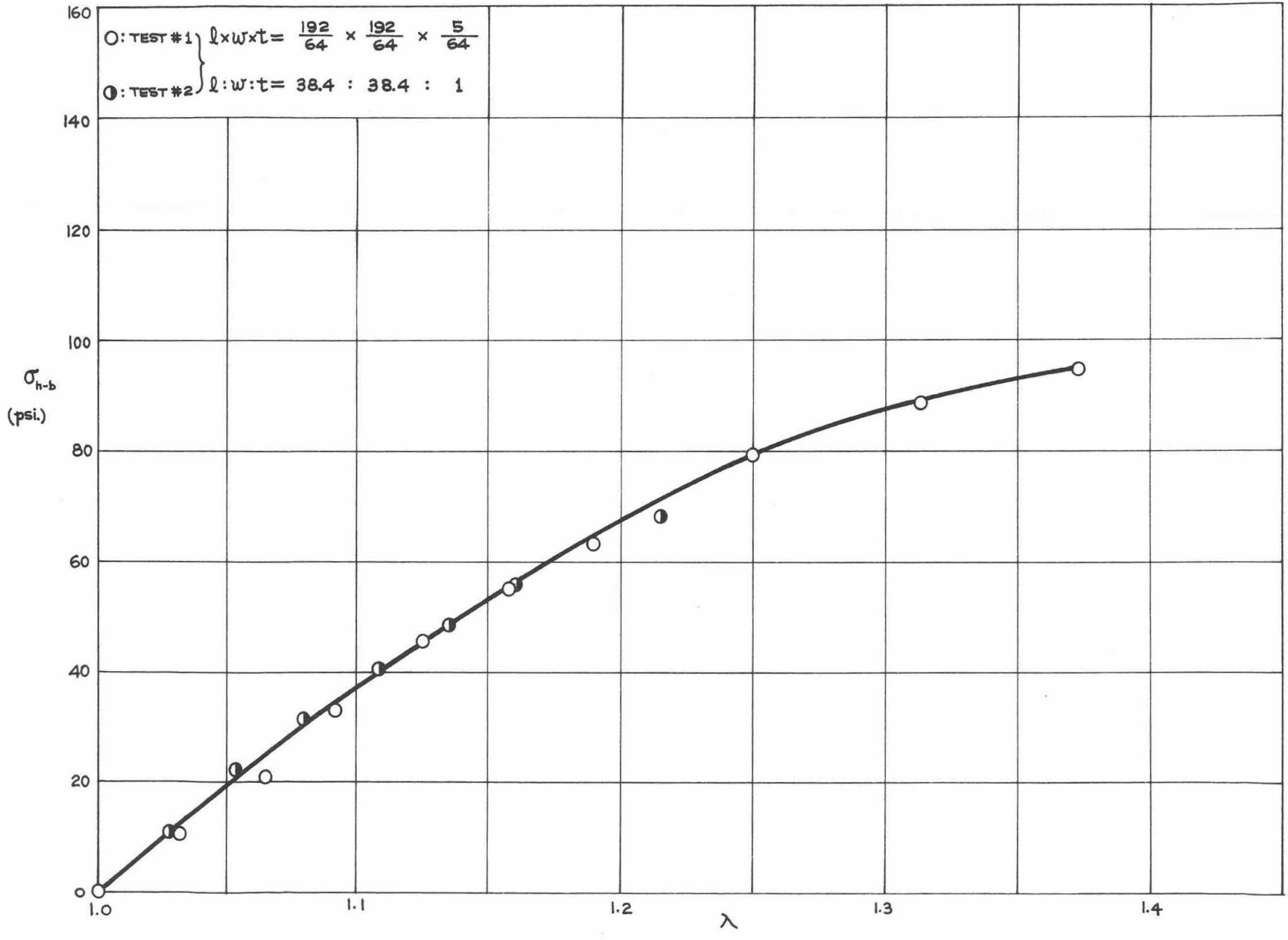

FIG. I.22. EVALUATION OF W_1 & W_2 FROM RECTIFIED HOMOGENEOUS-BIAXIAL DATA

SBR-1500 (3 % S)

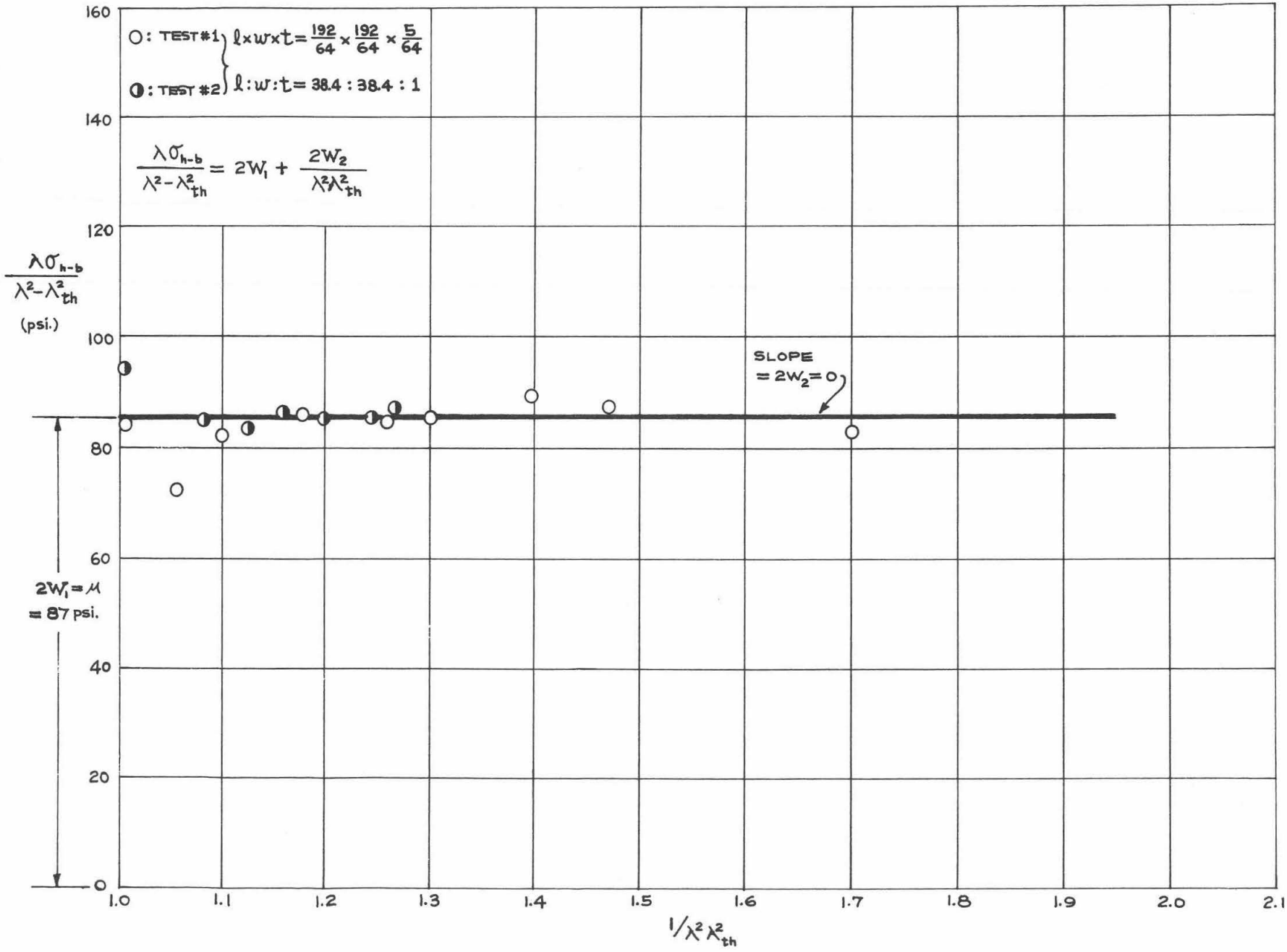

FIG.I.23. HOMOGENEOUS-BIAXIAL THICKNESS CONTRACTION RATIO VS. LONGITUDINAL EXTENSION RATIO

SBR-1500 (3 % S)

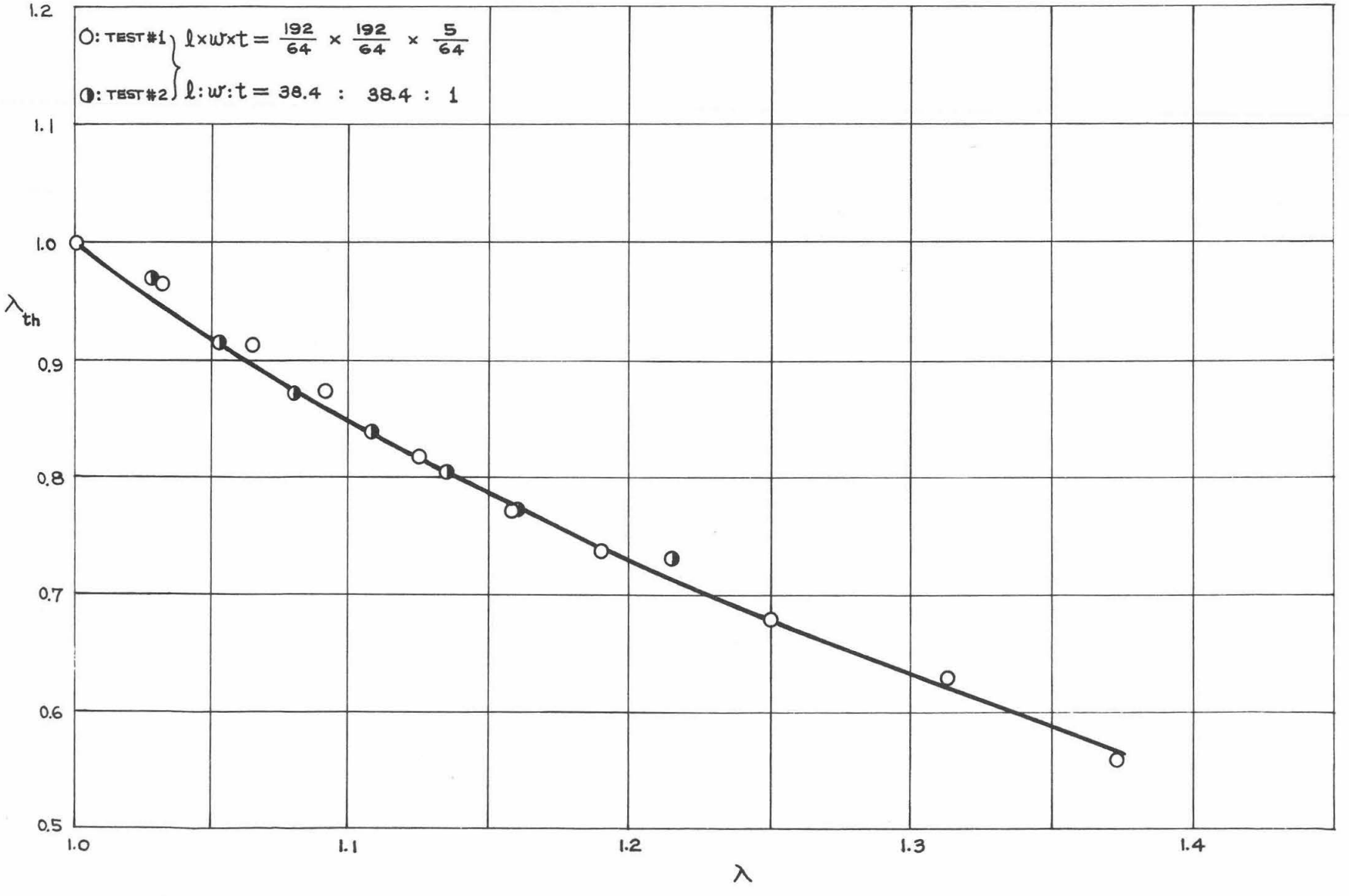

FIG. I.24. BIAXIAL STRESS VS. LONGITUDINAL EXTENSION RATIO

PU-FOAM

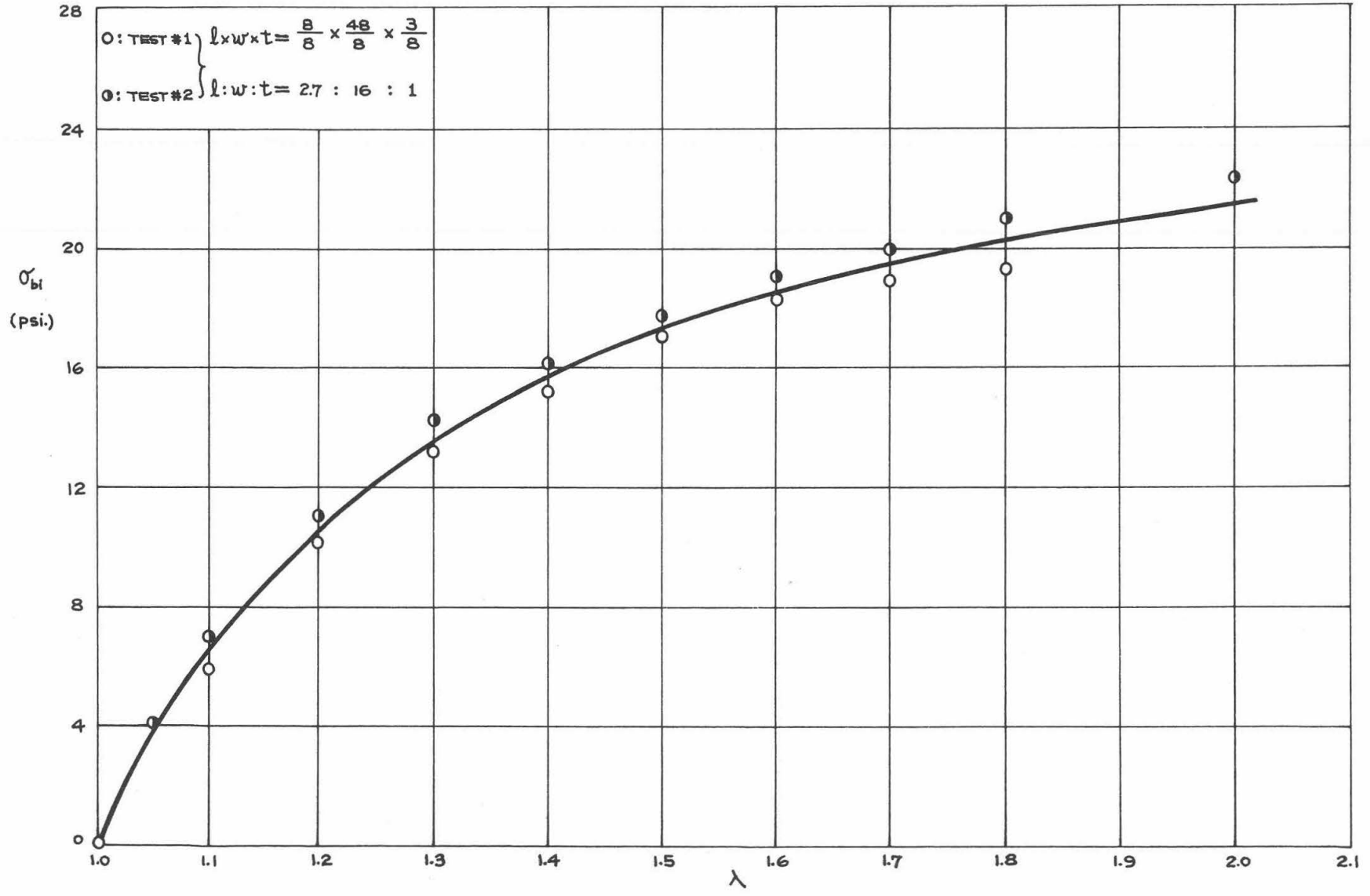

FIG.I.25. EVALUATION OF W_1 & W_2 FROM RECTIFIED BIAXIAL DATA

PU-FOAM

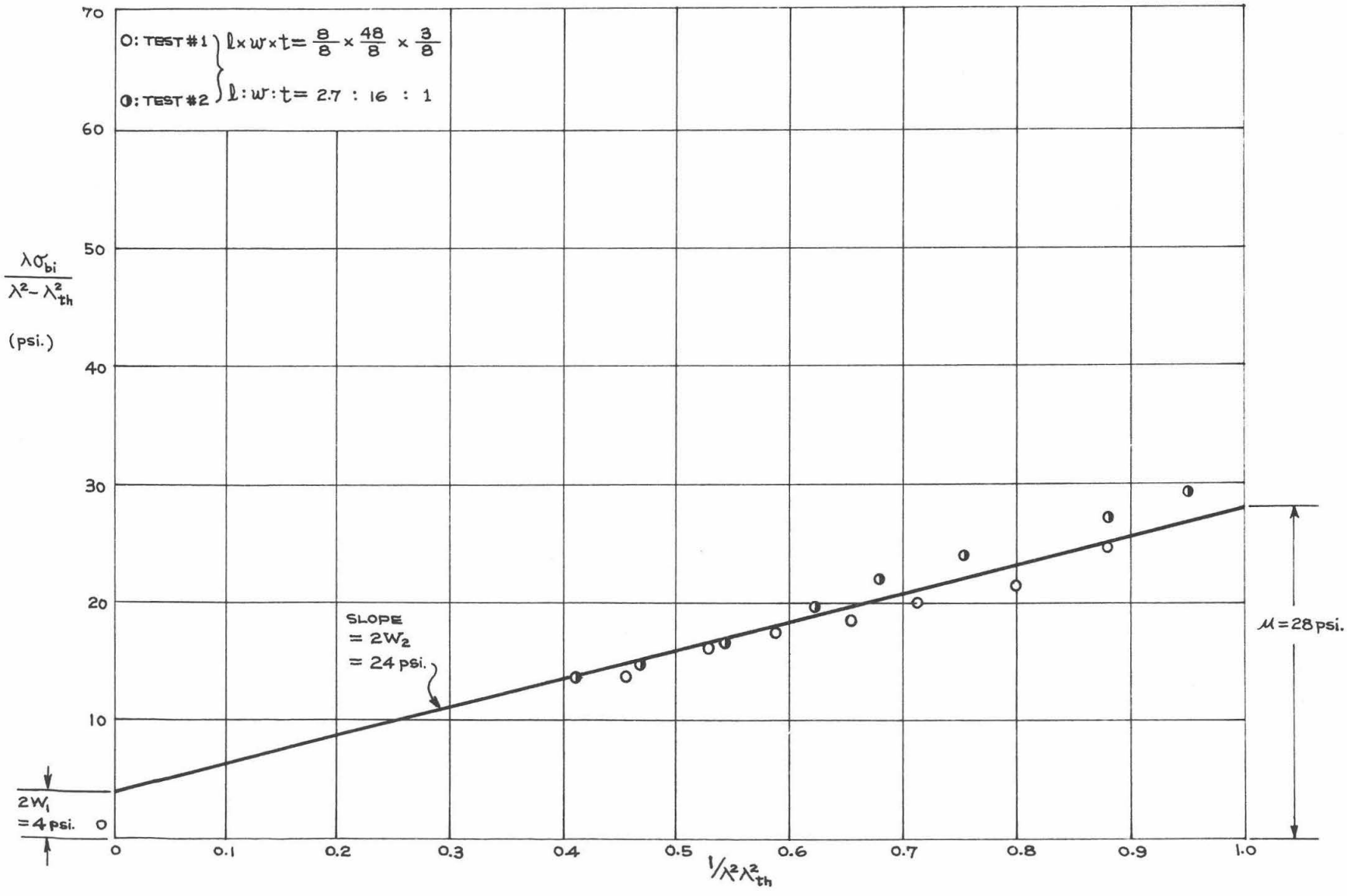

FIG. I.26. BIAXIAL THICKNESS CONTRACTION RATIO VS. LONGITUDINAL EXTENSION RATIO

PU-FOAM

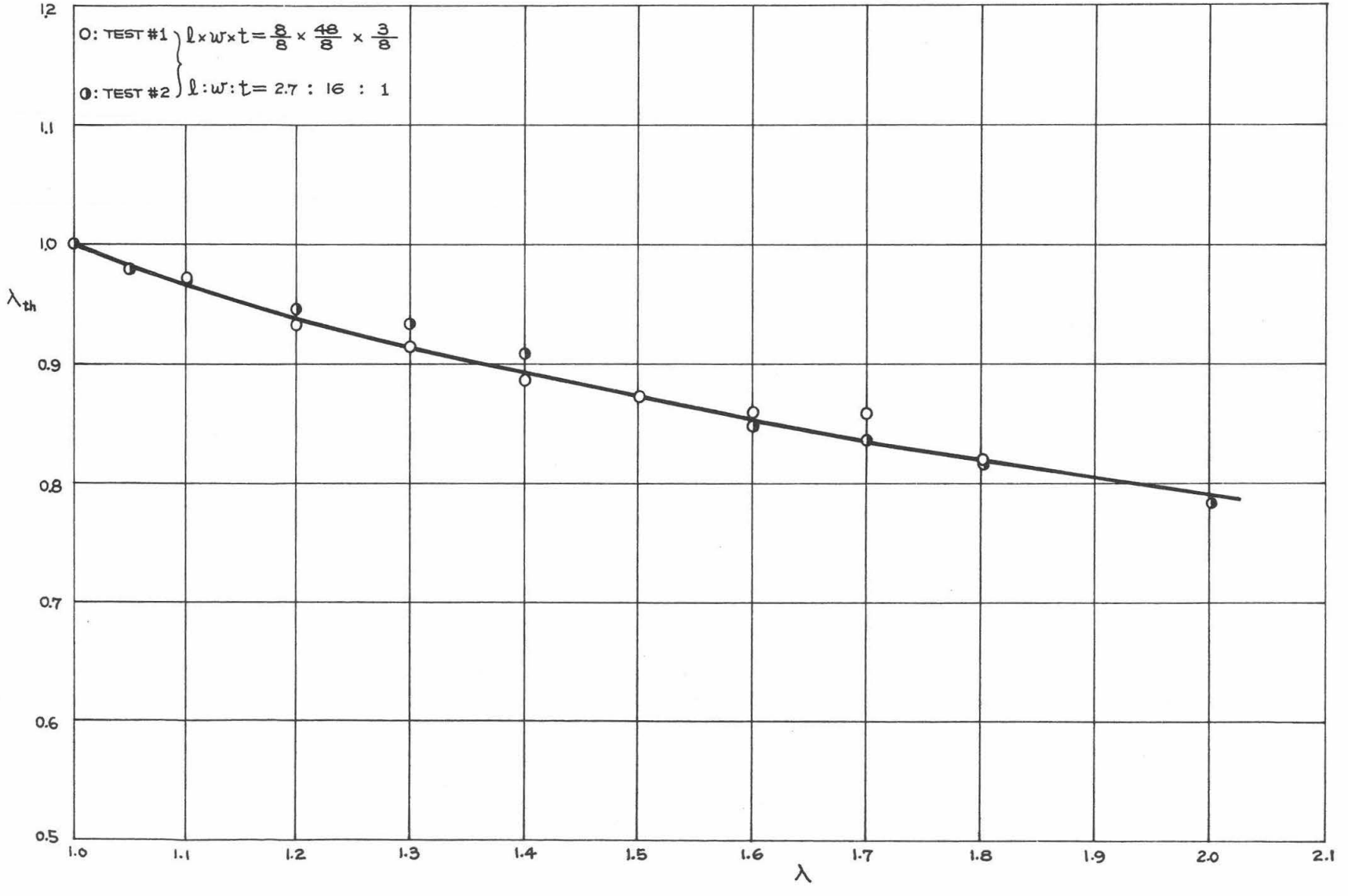

FIG.I.27. BIAXIAL DILATATION VS. LONGITUDINAL EXTENSION RATIO

P-U FOAM

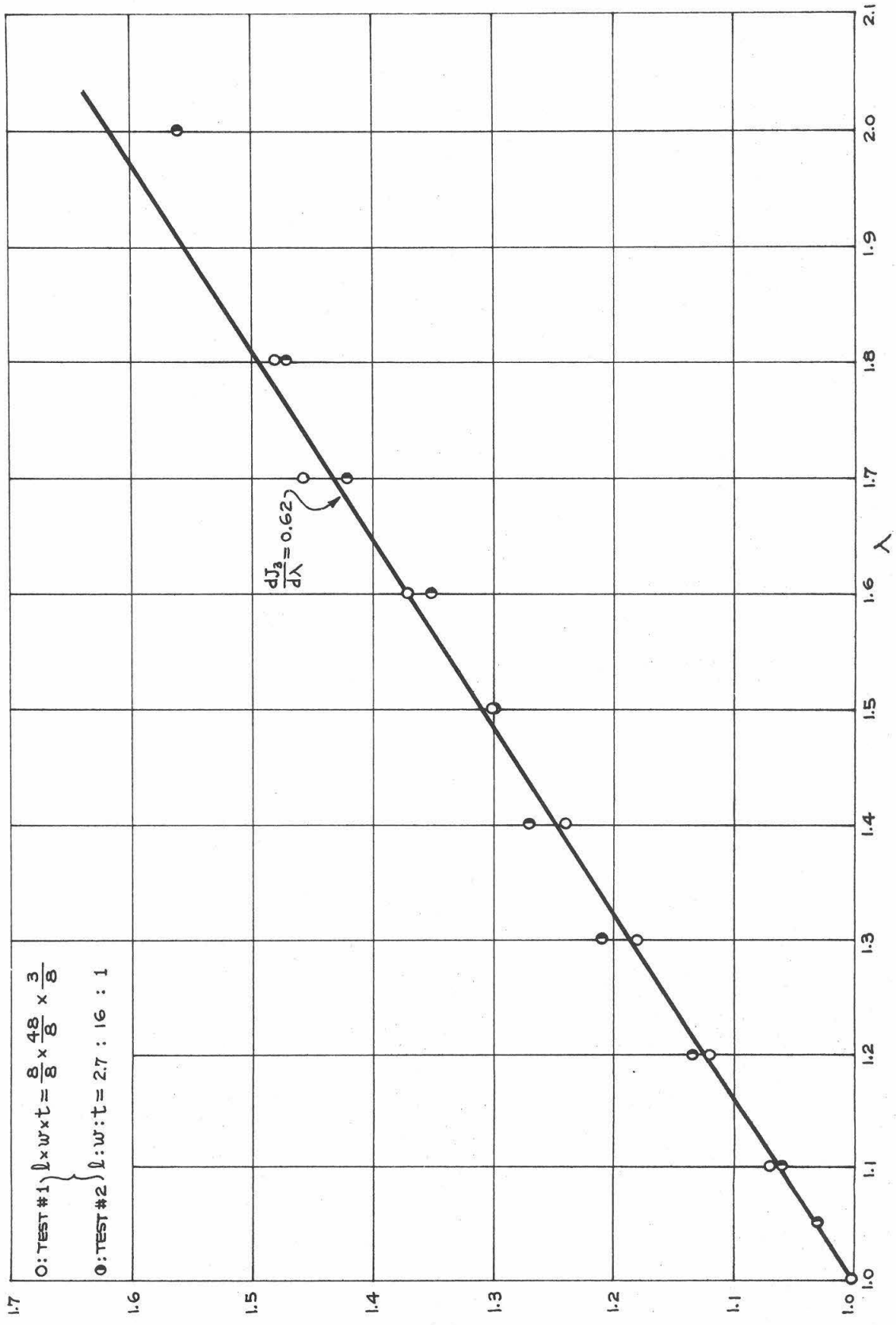

FIG.I.28. HOMOGENEOUS-BIAXIAL STRESS VS. LONGITUDINAL EXTENSION RATIO

PU-FOAM

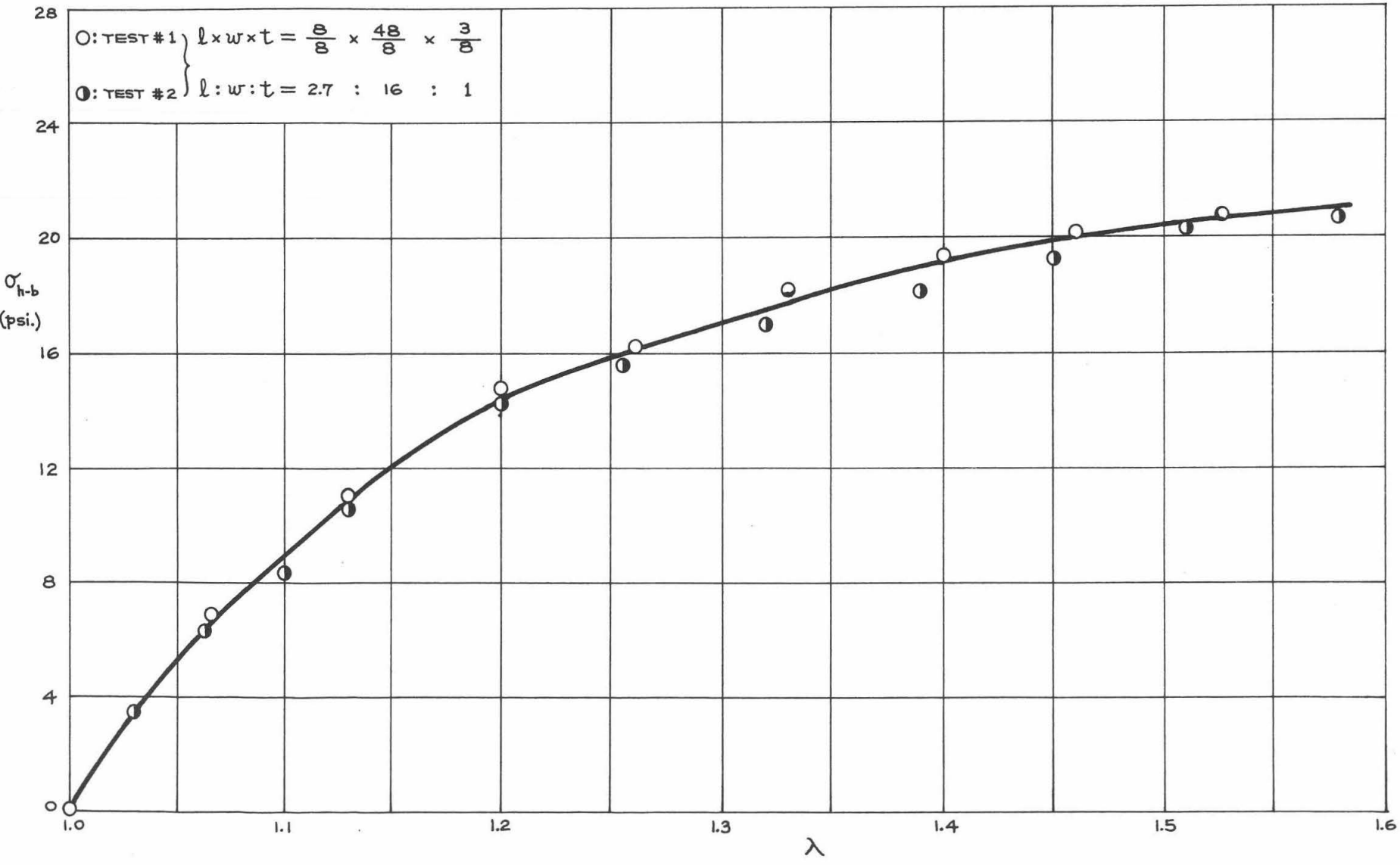

FIG. I.29. EVALUATION OF W_1 & W_2 FROM RECTIFIED HOMOGENEOUS-BIAXIAL DATA

PU-FOAM

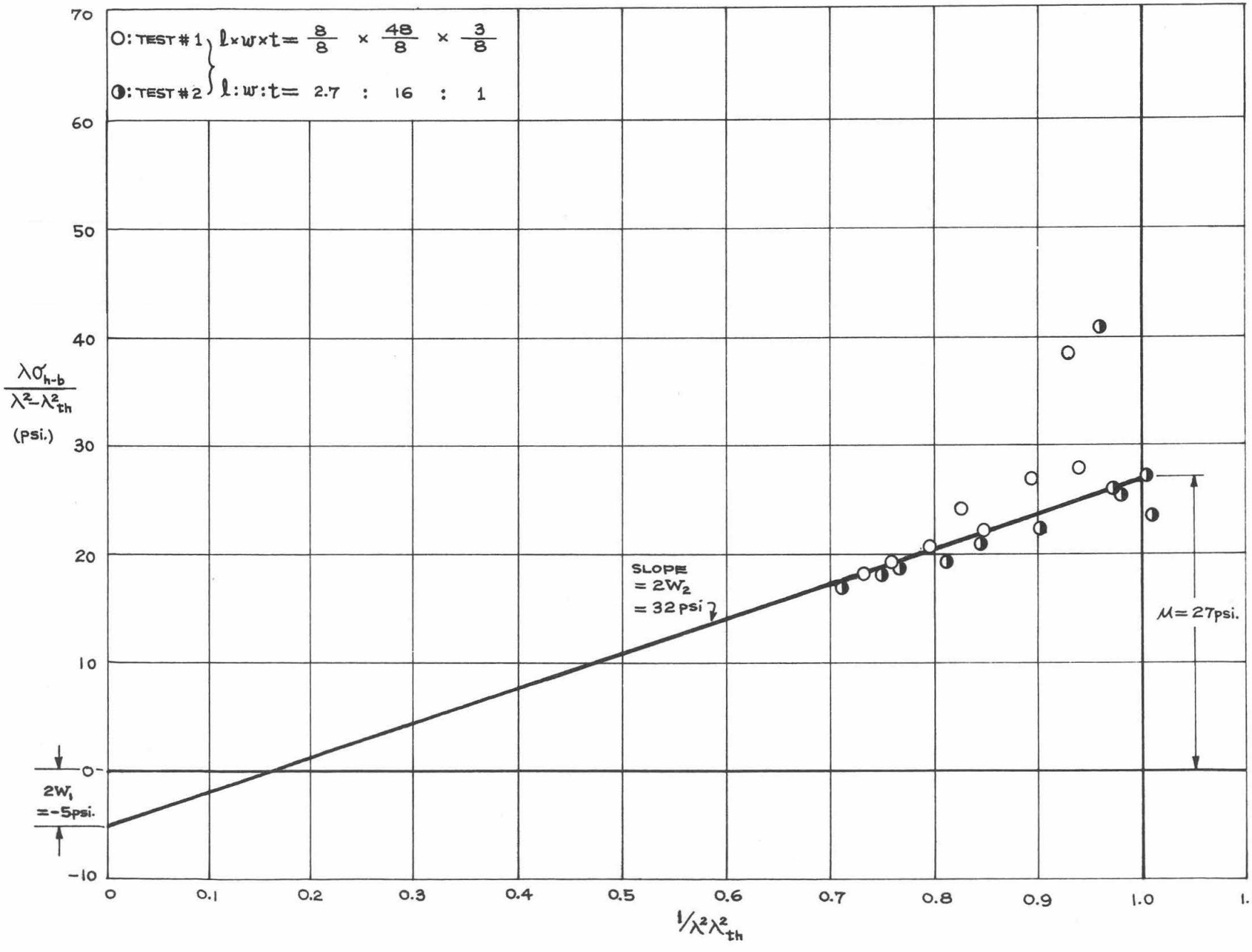

FIG. I.30. HOMOGENEOUS-BIAXIAL THICKNESS CONTRACTION RATIO VS. LONGITUDINAL EXTENSION RATIO

PU-FOAM

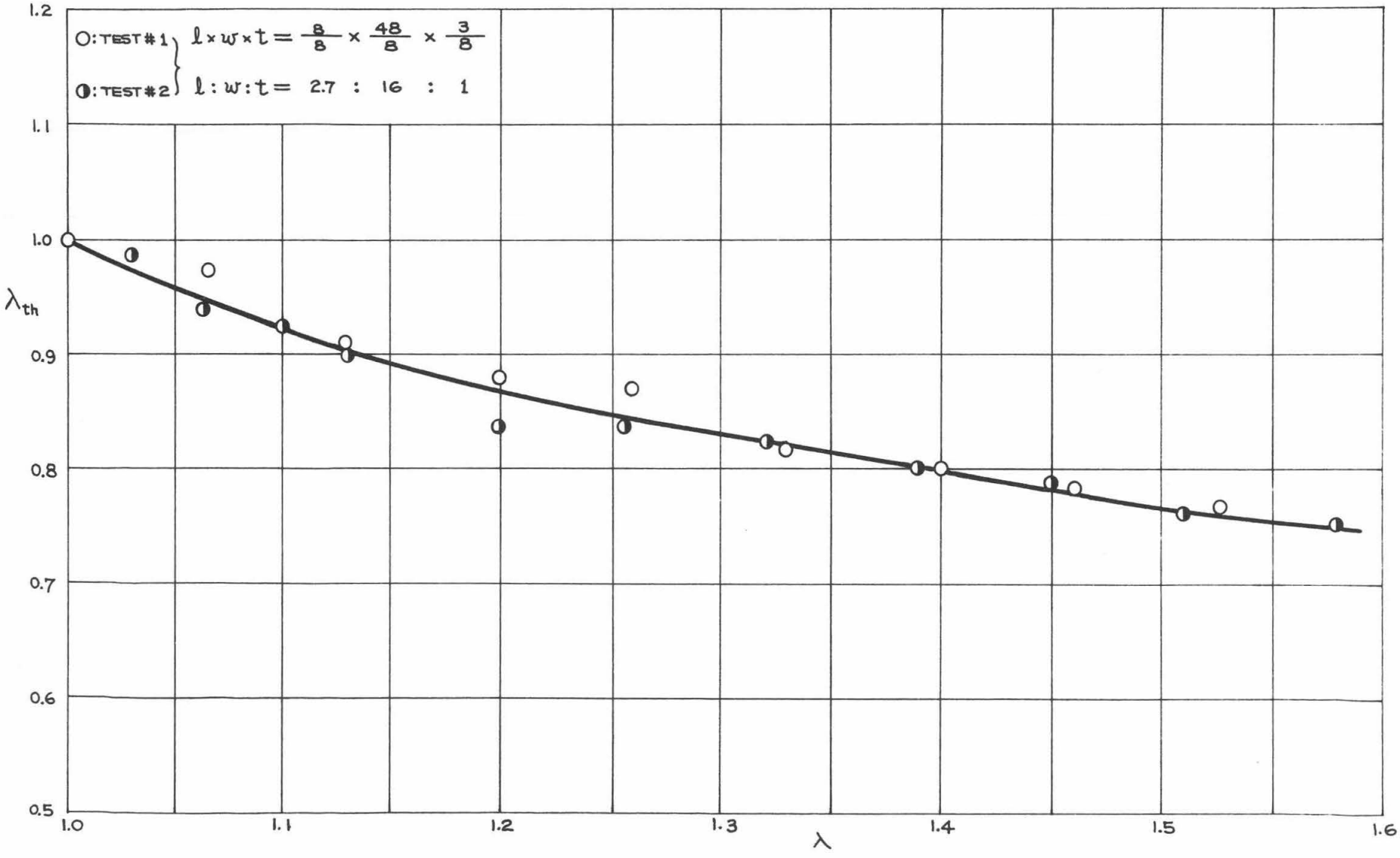

FIG. I.31. HOMOGENEOUS-BIAXIAL DILATATION VS. LONGITUDINAL EXTENSION RATIO

PU-FOAM

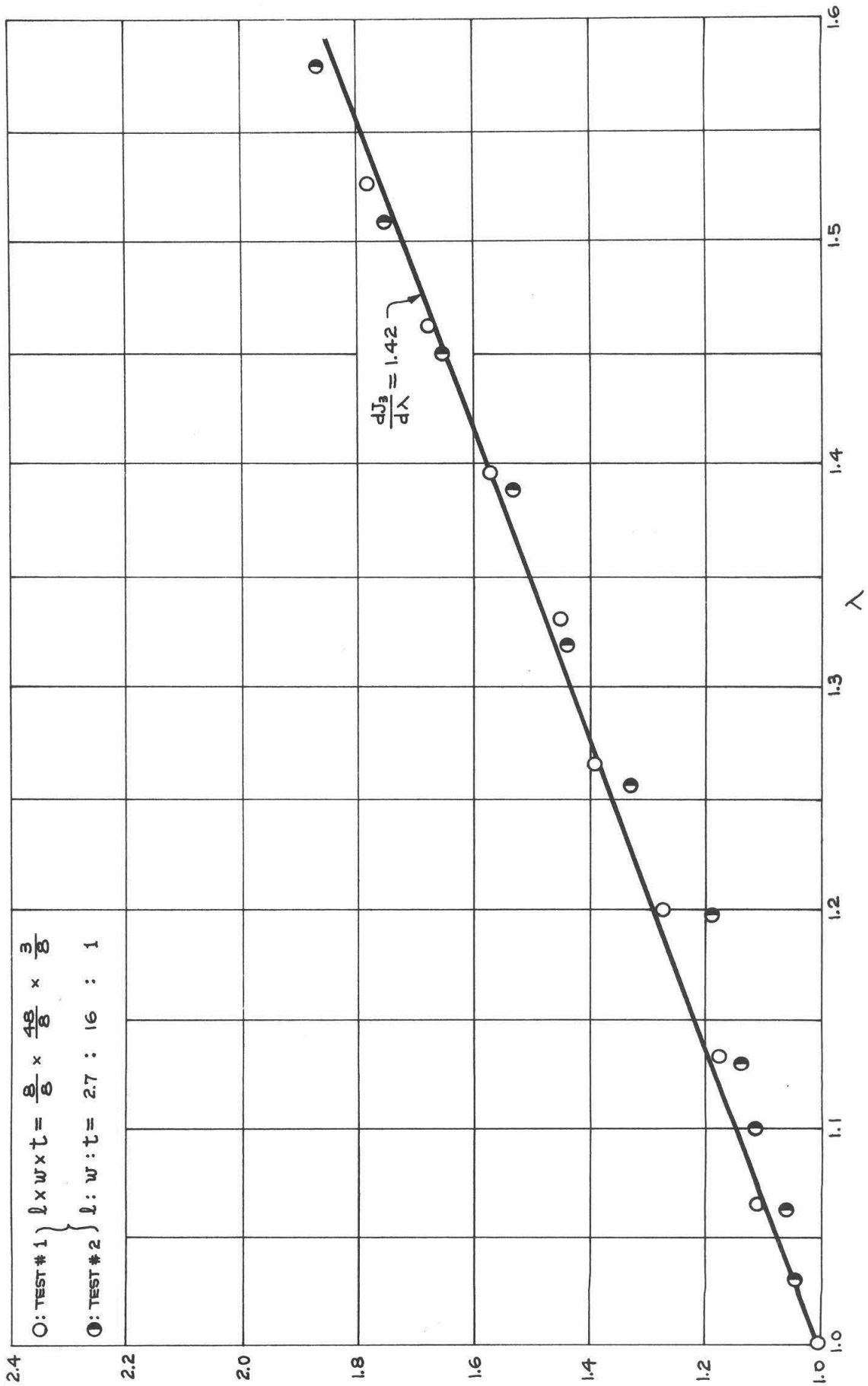

IV. STRESS ANALYSIS

A. Introduction

In the last quarterly report a discussion of the plane strain and/or plane stress deformation of an elastic sector-space was initiated. The stresses and displacements of the general elastic field were expressed in terms of a real potential ϕ , and also in terms of complex potentials ϕ and χ . For the case of clamped-free boundary conditions it was shown that one has to solve a pair of integral equations (Hilbert's problem) and that the roots of a characteristic polynomial (sometimes called eigen values) associated with the kernel of these equations are in general complex. Because of the importance of the nature of this polynomial we shall consider in this report a somewhat simpler algebraic problem in which the sector-space is subjected only to tangential stresses at the boundary. In this problem the analytic character of the stress-displacement field and its relation to the characteristic polynomial is easily displayed. A number of extremely interesting observations arise, which will prove useful in the elucidation of the mixed boundary value problem. The current problem is an extension of the free-free eigenvalue problem first studied by Knein and Williams.

B. The Tangentially Stressed Elastic Sector-Space

Consider an elastic sector-space of flank angle 2α , which is subjected to the following contact stresses at the boundaries

at $\theta = \pm\alpha$

$$\begin{aligned} \sigma_\theta &= -q_r \quad , \qquad 0 \le r \le a \\ \sigma_\theta &= 0 \quad , \qquad a < r \\ \tau_{r\theta} &= 0 \quad , \qquad 0 \le r < \infty \end{aligned} \tag{IV.1}$$

Since the boundary conditions are homogeneous, it is possible to use an operational transform. Integral equations arise only in the case of mixed boundary value problems, for which case techniques other than operational transform must be used. The choice of integral transform is dictated by the nature of the algebra. In the real variable field, it is most convenient to

use a Laplace transform; in the complex variable field, a Fourier transform. We choose the real variable field and Laplace transform.

Before transforming the biharmonic equation into a form which allows the transform of the stress function Φ to be expressed as an algebraic function of the boundary conditions and the angle θ, let us recall (GALCIT SM 61-15, IV. 19) that the biharmonic equation is considerably simplified by the introduction of the variable

$$s = \ln r \tag{IV. 2}$$

In terms of this new variable, the Laplace transform is of necessity two-sided, so that

$$\overline{\Phi} = \int_{-\infty}^{\infty} \Phi\, e^{-ps}\, ds \tag{IV. 3}$$

Thus it is necessary to know the conditions under which this integral converges and the analytic properties of $\overline{\Phi}$ in the complex plane, preparatory to solving the given problem. In fact the step-function boundary condition was chosen exactly with this thought in mind, namely, to guarantee convergence of the definition integral (IV. 3). Before discussing these properties let us cast (IV. 3) into its more familiar equivalent, the Mellin transform:

$$\overline{\Phi} = \int_{0}^{\infty} \Phi\, r^{p-1}\, dr \tag{IV. 4}$$

C. Properties of the Mellin Transform (or Two-Sided Laplace Transform)

1. Recursive Derivatives

In GALCIT SM 61-15, the biharmonic equation was expressed in terms of the radial variable as follows:

$$r^4\Phi_{rrrr} + 2r^3\Phi_{rrr} - r^2\Phi_{rr} + r\Phi_r + 2r^2\Phi_{rr\theta\theta} - 2r\Phi_{r\theta\theta} + 4\Phi_{\theta\theta} + \Phi_{\theta\theta\theta\theta} = 0 \tag{IV. 5}$$

In order to transform term by term with the Mellin operation we need the general expression for $r^n\Phi_{(rr\text{----}r)_{n\text{ times}}}$

Note that

$$\overline{r\Phi_r} = \int_0^\infty \Phi_r r^p dr = r\Phi\Big|_0^\infty - p\int_0^\infty \Phi\, r^{p-1}\, dr \tag{IV.6}$$

$$\overline{r\Phi_r} = -p\overline{\Phi} \tag{IV.7}$$

if

$$r^p\Phi\Big|_0^\infty = 0 \tag{IV.8}$$

This condition will be verified later in the Appendix A.
Note further that

$$\overline{r^2\Phi_{rr}} = \int_0^\infty \Phi_{rr}\, r^{p+1} dr = r^{p+1}\Phi_r\Big|_0^\infty + (p+1)p\overline{\Phi} \tag{IV.9}$$

$$\overline{r^2\Phi_{rr}} = (p+1)p\overline{\Phi} \tag{IV.10}$$

if

$$r^{p+1}\Phi_r\Big|_0^\infty = 0 \tag{IV.11}$$

(IV.11) is equivalent to (IV.8) within a constant factor, so that the condition at r=0 and r = ∞ will hold for all higher derivatives. It follows that

$$\overline{r^n\Phi_{(r---r)_{n\text{ times}}}} = (-1)^n \frac{(p+n-1)!}{(p-1)!}\overline{\Phi} \tag{IV.12}$$

2. Analytic Properties of the Inversion Integral

Assume now that the definition integral $\overline{\Phi}$ exists and is analytic in a strip $a < \mathrm{Re}(p) < b$, then the inversion integral is given by

(IV.13)

It is readily shown * that the following conditions are necessary and sufficient for the existence of this integral:

$$\text{a.} \quad \int_{-\infty}^{\infty} \left| \overline{\Phi}(x+iy) \right| dy \qquad \text{converges for } a < x < b \tag{IV.14}$$

$$\text{b.} \quad \lim_{y \to \infty} \overline{\Phi}(x+iy) \to 0 \qquad \text{, uniformly in the strip, } a < x < b \tag{IV.15}$$

$$\text{c.} \quad r \text{ real and positive} \tag{IV.16}$$

Condition c follows from the geometry of the problem. Condition a and b will be verified in the Appendix B. In addition we must specify the boundaries of the strip[a, b]

D. Application of the Transform

Using (IV. 12), (IV. 5) becomes

$$(p+2)^2 p^2 \overline{\Phi} + [(p+2)^2 + p^2] \overline{\Phi}_{\theta\theta} + \overline{\Phi}_{\theta\theta\theta\theta} = 0 \tag{IV.17}$$

the general solution of which is given by:

$$\overline{\Phi} = A \sin p\theta + B \cos p\theta + C \sin (p+2)\theta + D \cos (p+2)\theta \tag{IV.18}$$

Because $\theta = 0$ defines a plane of symmetry, $\overline{\Phi}$ must be an even function of θ :

$$\overline{\Phi} = B \cos p\theta + D \cos (p+2)\theta \tag{IV.19}$$

We also have:

$$\overline{r^2 \sigma_\theta} = \overline{r^2 \Phi_{rr}} = (p+1) p \overline{\Phi} \tag{IV.20}$$

$$\overline{r^2 \sigma_r} = \overline{r \Phi_r} + \overline{\Phi_{\theta\theta}} = \overline{\Phi_{\theta\theta}} - p\overline{\Phi} \tag{IV.21}$$

$$\overline{r^2 \tau_{r\theta}} = (p+1) \overline{\Phi_\theta} \tag{IV.22}$$

---

* McLachlan, N. W.: Complex Variable and Operational Calculus. University Press, p. 302 (1944).

At $\theta = \pm \alpha$, (IV. 20) becomes

$$-q\int_0^a r^{p+1}dr = -q\frac{a^{p+2}}{p+2} = (p+1)p\left[B\cos p\alpha + D\cos(p+2)\alpha\right] \qquad \text{(IV. 23)}$$

At $\theta = \pm \alpha$, (IV. 22) becomes

$$0 = -BP\sin p\alpha - D(p+2)\sin(p+2)\alpha \qquad \text{(IV. 24)}$$

Solution for B and D and insertion into (IV. 19) yields

$$\overline{\Phi}(p) = -\frac{q a^{p+2}}{(p+2)(p+1)p}\,\frac{(p+2)\sin(p+2)\alpha\cos p\theta - p\sin p\alpha\cos(p+2)\theta}{(p+2)\sin(p+2)\alpha\cos p\alpha - p\sin p\alpha\cos(p+2)\alpha} \qquad \text{(IV. 25)}$$

It is more convenient to deal with

$$\overline{\Phi}(p-1) = -\frac{q a^{p+1}}{(p+1)p(p-1)}\,\frac{(p+1)\sin(p+1)\alpha\cos(p-1)\theta - (p-1)\sin(p-1)\alpha\cos(p+1)\theta}{E(p,\alpha)} \qquad \text{(IV. 26)}$$

where $E(p,\alpha) = (p+1)\sin(p+1)\alpha\cos(p-1)\alpha - (p-1)\sin(p-1)\alpha \times$

$$\times\cos(p+1)\alpha = p\sin 2\alpha + \sin 2p\alpha \qquad \text{(IV. 27)}$$

The polynomial E is characteristic of free-free problems. But it is not by any means to be inferred that its roots <u>alone</u> determine the nature of the stress field obtained from the inversions of (IV. 26), (IV. 20), (IV. 21), (IV. 22). In order to see this let us now examine the inversion integral.

E. Poles of the Inversion Integral

From (IV. 13), we have

$$-\frac{\Phi(r)}{q a^2} = \frac{1}{2\pi i}\int_{c-i\infty}^{c+i\infty}\frac{(p+1)\sin(p+1)\alpha\cos(p-1)\theta - (p-1)\sin(p-1)\alpha\cos(p+1)\theta}{(p+1)p(p-1)\,E(p,\alpha)}\left(\frac{a}{r}\right)^{p-1}dp \qquad \text{(IV. 28}$$

$$a < c < b$$

The integrand of (IV. 28) has simple poles at +1, 0, -1 and in addition, simple poles located at the non-zero roots of $E(p, \alpha)$. It is easily shown by application of L'Hopital's rule that the zero root of $E(p, \alpha)$ is cancelled out by a zero of the same order in the numerator of the integrand.

The non-zero roots of $E(p, \alpha) = p \sin 2\alpha + \sin 2p\alpha = 0$ are identified as follows: Let

$$2p\alpha = \beta + i\gamma \tag{IV.29}$$

$$\frac{\sin 2\alpha}{2\alpha} = k \tag{IV.30}$$

from which $$\sin(\beta + i\gamma) = -k(\beta + i\gamma) \tag{IV.31}$$

$$\cosh\gamma = -\frac{k\beta}{\sin\beta} \tag{IV.32}$$

$$\cos\beta = -\frac{k\gamma}{\sinh\gamma} \tag{IV.33}$$

Note the minus sign in all three of the preceding equations. In Williams' * paper the plus and minus sign would correspond to a more general, non-symmetric loading.

Note first the behavior of $k \equiv \frac{\sin 2\alpha}{2\alpha}$ as a function of 2α in Figure IV. 1. From $0 < 2\alpha < \pi$, k is a positive fraction bounded by unity; from $\pi < 2\alpha < 2\pi$ k is a negative fraction bounded by -. 218. Thus if $k > .218$ which implies $0 < 2\alpha < 147^{\circ}$, non-zero real roots cannot exist because (IV. 31) would reduce to

$$\frac{\sin\beta}{\beta} = -k < -.218 \tag{IV.34}$$

This corresponds to the arbitrary horizontal line designated (A) on Figure IV. 1. In order to determine the complex values of the roots, we continue with the hypothesis $k > .218$ (the cases $k < .218$ will be discussed subsequently),

---

* Williams, M. L.: "Stress Singularities Resulting from Various Boundary Conditions in Angular Corners of Plates in Extension." Journal of Applied Mechanics, Vol. 19, 1952.

and note, as β is increased beyond $2\alpha = 147^{\circ}$, and thereby approaches π, that $\frac{\sin\beta}{\beta}$ remains positive, and therefore that (IV.31) cannot be satisfied since the hyperbolic cosine is positive definite. On the other hand, as β is increased beyond π, $\frac{\sin\beta}{\beta}$ becomes negative. For convenience, we set

$$\beta = \pi + \epsilon \ , \text{ with } \ \epsilon > 0 \tag{IV.35}$$

$$\sin\beta = -\sin\epsilon = -\epsilon + \frac{\epsilon^3}{6} \tag{IV.36}$$

$$\cos\beta = -\cos\epsilon = -1 + \frac{\epsilon^2}{2} \tag{IV.37}$$

by (IV.32)
$$\cosh\gamma = \frac{-k(\pi+\epsilon)}{-\epsilon + \frac{\epsilon^2}{6}} \approx \frac{k\pi}{\epsilon} \ , \text{ a large number} \tag{IV.38}$$

$$\gamma = \pm \ln\left[\frac{k\pi}{\epsilon} + \sqrt{\frac{k^2\pi^2}{\epsilon^2} - 1}\ \right] \tag{IV.39}$$

$$\sinh\gamma = \pm\sqrt{\frac{k^2\pi^2}{\epsilon^2} - 1} \tag{IV.40}$$

by (IV.33)
$$\cos\beta = -k\,\frac{\ln\left[\frac{k\pi}{\epsilon} + \sqrt{\frac{k^2\pi^2}{\epsilon^2} - 1}\ \right]}{\sqrt{\frac{k^2\pi^2}{\epsilon^2} - 1}} \approx -\frac{\epsilon}{\pi}\ln\left(\frac{2k\pi}{\epsilon}\right) \tag{IV.41}$$

Since (IV.41) must equal (IV.37) ϵ cannot be small because

$$\epsilon \ln\epsilon \to 0 \ , \text{ as } \quad \epsilon \to 0 \tag{IV.42}$$

This suggests that we should let β increase further toward $\frac{3\pi}{2}$. We set

$$\beta = \frac{3\pi}{2} - \epsilon \tag{IV.43}$$

$$\sin\beta = -\cos\epsilon = -1 + \frac{\epsilon^2}{2} \tag{IV.44}$$

$$\cos\beta = -\sin\epsilon = -\epsilon + \frac{\epsilon^3}{6} \tag{IV.45}$$

by (IV.32)
$$\cosh\gamma = \frac{-k\left(\frac{3\pi}{2} - \epsilon\right)}{-1 + \frac{\epsilon^2}{2}} = \frac{3\pi k}{2} \tag{IV.46}$$

$$\gamma = \pm \ln\left[\frac{3\pi k}{2} + \sqrt{\frac{9\pi^2k^2}{4} - 1}\right] \tag{IV.47}$$

$$\sinh\gamma = \pm\sqrt{\frac{9\pi^2k^2}{4} - 1} \tag{IV.48}$$

by (IV.33)
$$\cos\beta = -k\,\frac{\ln\left[\frac{3\pi k}{2} + \sqrt{\frac{9\pi^2k^2}{4} - 1}\right]}{\sqrt{\frac{9\pi^2k^2}{4} - 1}} \approx -\frac{2}{3\pi}\ln(3\pi k) \tag{IV.49}$$

by (IV.45)
$$\epsilon = k\,\frac{\ln\left[\frac{3\pi k}{2} + \sqrt{\frac{9\pi^2k^2}{4} - 1}\right]}{\sqrt{\frac{9\pi^2k^2}{4} - 1}} \approx \frac{2}{3\pi}\ln(3\pi k) \tag{IV.50}$$

so that, to an excellent approximation

$$2\alpha p_o = \frac{3\pi}{2} - k\,\frac{\ln\left[\frac{3\pi k}{2} + \sqrt{\frac{9\pi^2k^2}{4} - 1}\right]}{\sqrt{\frac{9\pi^2k^2}{4} - 1}} \pm i\ln\left[\frac{3\pi k}{2} + \sqrt{\frac{9\pi^2k^2}{4} - 1}\right] \tag{IV.51}$$

By retaining higher powers of ϵ it is a simple matter to compute the exact values of the lowest conjugate roots p_o. For example, in the case

$2\alpha = \frac{\pi}{6} = 30^{o}$, the exact values of p_o are $8.04 \pm 4.19\ i$, whereas the approximations given by (IV.51) are $p_o = 8.09 \pm 4.18\ i$. This first intersection is demonstrated by the point (B) on the horizontal line (B, C, D) in Figure IV.1. It is readily demonstrated that the higher roots are given by

$$p_m = \frac{(4m+3)\frac{\pi}{2} \pm i \ln (4m+3)\pi k}{2\alpha} \qquad m = 1, 2, 3 \text{ etc.} \tag{IV.52}$$

All higher roots given by (IV.52) are within a few hundredths of one percent of the exact solutions. Note further that (IV.31) is an even function of β, so that (IV.52) reflects into the negative real plane to give:

$$p_m = \pm \frac{(4m+3)\frac{\pi}{2} \pm i \ln (4m+3)\pi k}{2\alpha} \qquad m = 1, 2, 3 \text{ etc.} \tag{IV.53}$$

where the respective $\pm$ symbols in (IV.53) are uncoupled. If further (IV.53) is extended back to m = 0, the lowest roots are given by

$$p_o = \pm 9 \pm 4.18\ i \tag{IV.54}$$

which represents only a 12 percent error in the real part. For the purpose of simplicity, this error will be subsumed in the following discussion.

In recapitulation, the roots of $E(p, \alpha) = 0$ are given by

$$p = -1,\ 0,\ 1 \text{ and by equation (IV.53)} \tag{IV.55}$$

However for completeness it should be added here that when angle α is such that $k \leq 0.218$ then real roots other than $p = -1,\ 0,\ 1$ of $E(p, \alpha) = 0$ are possible. The number of these real roots will increase and decrease as increases. Two special cases should be noted, $\alpha = \pi/2$ and $\alpha = \pi$; for these values of α there will be no complex roots but there will be an infinite number of real roots. This can be easily seen from equations (IV.32) and (IV.33).

F. Determination of the Strip Boundaries a, b for the Case $2\alpha = 30^{\circ}$

Figure IV.2 shows a schematic plot of the possible locations of path c amidst the poles of the integrand of (IV.28) in the complex plane (only the lowest pairs of conjugates $p_m = p_o$ are included). Possible locations of path c are designated by roman numerals I - IV, where the left and right bounds of each path include the nearest poles in the horizontal sense. Note that no consideration is given to paths which interlace the non-zero roots of $E(p, \alpha) = 0$, for reasons which will be developed later on. Choosing c to be path I, as a start, we can evaluate (IV.28) formally by completing a Cauchy contour counter-clockwise for $r < a$ and clockwise * for $r > a$. Thus we have

For $r < a$

$$-\frac{\Phi_I}{q_f a^2} = \frac{1}{2} - \frac{r}{a}\,\frac{\sin\alpha\cos\theta + \theta\sin\alpha\sin\theta + \alpha\cos\alpha\cos\theta}{\alpha + \sin\alpha\cos\alpha} + \frac{r^2}{2a^2}$$

$$+\sum_{m=o}^{\infty} \frac{(p_m+1)\sin(p_m+1)\alpha\cos(p_m-1)\theta - (p_m-1)\sin(p_m-1)\alpha\cos(p_m+1)\theta}{(p_m+1)p_m(p_m-1)(\sin 2\alpha + 2\alpha\cos 2p_m\alpha)}\left(\frac{r}{a}\right)^{1-p_m}$$

$$\text{where} \qquad 2\alpha p_m = -(4m+3)\frac{\pi}{2} \pm i\,\ln(4m+3)\pi k \qquad \text{(IV.56)}$$

The first term on the right hand side is generated by the pole at $p = 1$, the second term from the pole $p = 0$, and the third from the pole $p = -1$.

For $r > a$

$$-\frac{\Phi_I}{q_f a^2} = -\sum_{m=o}^{\infty} \frac{(p_m+1)\sin(p_m+1)\cos(p_m-1)\theta - (p_m-1)\sin(p_m-1)\alpha\cos(p_m+1)\theta}{(p_m+1)p_m(p_m-1)(\sin 2\alpha + 2\alpha\cos 2p_m\alpha)}\left(\frac{r}{a}\right)^{1-p_m}$$

$$\text{where} \qquad 2\alpha p_m = (4m+3)\frac{\pi}{2} \pm i\,\ln(4m+3)\pi k \qquad \text{(IV.57)}$$

---

* Note: In each case it is very easy to prove from elementary complex variable theory, that the integral along the Cauchy contour is equal to zero.

Equation (IV.56), (IV.57) gives a complete description of the stress function over the range $0 < r < a < r < \infty$, evaluated from the inversion integral taken along path I. Since the real part of the lowest order conjugate pole is equal to -8 in the range $r < a$, it follows that the earliest contributions from the sum in this range are of the order $(r/a)^9$; this is negligible with respect to $(\frac{r}{a})^2$ when $r \ll a$. Even when $r = a$, the sum is still negligible; direct calculation indicates it does not exceed 2 percent of the value of the pole at negative unity. The sum argument applies when $r > a$, since then the real front of the lowest conjugate lies in the right half plane and is equal to 8.04. Thus equations (IV.56) (IV.57) may be well approximated by the representation

$$-\frac{\Phi_I}{qa^2} = \frac{1}{2} - \frac{r}{a}\frac{\sin\alpha\cos\theta + \theta\sin\alpha\sin\theta + \alpha\cos\alpha\cos\theta}{\alpha + \sin\alpha\cos\alpha} + \frac{1}{2}\left(\frac{r}{a}\right)^2 \qquad r<a \qquad \text{(IV.58)}$$

$$-\frac{\Phi_I}{qa^2} = 0 \qquad r>a \qquad \text{(IV.59)}$$

Before proceeding to evaluate the stresses and displacements corresponding to Φ_I, note that the pole at positive unity merely contributes a constant to the stress function. This has no physical bearing on the problem, so that paths I and II may be confluxed, ie, c can jump over the pole at + 1, and the strip $[a, b]_I$ is widened to extend from the root at zero to the complex roots at $(8.04 \pm 4.19\,i)$. Note further that

$$\text{at } \theta = \pm\alpha \qquad -\frac{\Phi_I}{qa^2} = \begin{cases} \frac{(a-r)^2}{2a^2}, & r<a \\ 0, & r>a \end{cases} \qquad \text{(IV.60)}$$

(IV.61)

which corresponds physically to the fact that the tangential load is applied only over the range $0 < r < a$.

Direct calculation yields, for $r < a$

$$\tau_{r\theta} = 0 \tag{IV.62}$$

$$-\frac{\sigma_\theta}{q} = 1 \tag{IV.63}$$

$$-\frac{\sigma_r}{q} = 1 - \frac{a}{r}\,\frac{2\sin\alpha\cos\theta}{\alpha+\sin\alpha\cos\alpha} \tag{IV.64}$$

$$-\frac{2\mu u}{q} = (1-2\sigma)r - (1-\sigma)a\ln r\,\frac{2\sin\alpha\cos\theta}{\alpha+\sin\alpha\cos\alpha} - a(1-2\sigma)\,\frac{\theta\sin\theta\sin\alpha}{\alpha+\sin\alpha\cos\alpha} \tag{IV.65}$$

$$-\frac{2\mu v}{q} = (1-\sigma)\,a\ln r\,\frac{2\sin\alpha\sin\theta}{\alpha+\sin\alpha\cos\alpha} - a(1-2\sigma)\,\frac{\theta\cos\theta\sin\alpha}{\alpha+\sin\alpha\cos\alpha} + a\,\frac{\sin\alpha\sin\theta}{\alpha+\sin\alpha\cos\alpha} \tag{IV.66}$$

and leads to all stresses and displacements equal to zero, for $r > a$. This means that, to the approximation suggested by (IV.59), the part of the wedge beyond "a" may be completely detached. This implies that the reaction load which balances the tangential force + $2q$ a sin (in the positive radial direction) must be concentrated at the apex $r = 0$, and this explains the existence of the singularity in σ_r. The force balance on the apex is as follows:

$$0 = -\int_0^a 2\sigma_\theta \sin\alpha\, dr + 2\int_0^\alpha (\sigma_r r)_a \cos\theta\, d\theta + \frac{\text{REACTION LOAD}}{\text{UNIT THICHNESS}} \tag{IV.67}$$

$$0 = 2qa\sin\alpha + 2qa\int_0^\alpha \left[1 - \frac{2\sin\alpha\cos\theta}{\alpha+\sin\alpha\cos\alpha}\right]\cos\theta\, d\theta + \text{REACTION} \tag{IV.68}$$

$$0 = \frac{4qa\sin\alpha}{\alpha+\sin\alpha\cos\alpha}\int_0^\alpha \cos^2\theta\, d\theta + \text{REACTION} \tag{IV.69}$$

$$\text{REACTION} = -2q\sin\alpha\,, \qquad \text{as predicted} \tag{IV.70}$$

Since the reaction load arises from the singular term in the radial stress, it follows that the logarithmic singularities in the displacements arise also from this concentrated force at the apex of the wedge. Furthermore, because of the singularity in the radial stress, infinitely large strains are predicted which are outside the province of linear theory, so that the expression (IV. 65) and (IV. 66) are to be considered as representative of the typical inconsistencies that arise when linear theory is used to express a singular strain field.

Turning now to path III, we immediately observe to the same approximation as used before, namely, neglecting the sums, that:

$$-\frac{\Phi_{III}}{qa^2} = \begin{cases} \dfrac{r^2}{2a^2}\,, & r<a \qquad \text{(IV.71)} \\[2ex] -\dfrac{1}{2}+\dfrac{r}{a}\,\dfrac{\sin\alpha\cos\theta+\theta\sin\alpha\sin\theta+\alpha\cos\alpha\cos\theta}{\alpha+\sin\alpha\cos\alpha}\,, & r>a \qquad \text{(IV.72)} \end{cases}$$

where the sign of the residues which correspond to the poles located at zero and positive unity are changed because the contour for $r > a$ is taken in the opposite sense to that for $r < a$.

Direct calculation yields, for $r < a$

$$\sigma_\theta = \sigma_r = -q\,, \qquad \tau_{r\theta} = 0 \tag{IV.73}$$

$$-\frac{2\mu u}{q} = r(1-2\sigma) \tag{IV.74}$$

$$-\frac{2\mu v}{q} = 0 \tag{IV.75}$$

This corresponds to a purely two-dimensional hydrostatic field. On the other hand for $r > a$, we have:

$$\sigma_\theta = \tau_{r\theta} = 0 \tag{IV.76}$$

$$-\frac{\sigma_r}{q} = \frac{2\sin\alpha\cos\theta}{\alpha + \sin\alpha\cos\alpha}\left(\frac{a}{r}\right) \tag{IV.77}$$

$$-\frac{2\mu u}{q} = \left[-(1-\sigma)a\ln r\cos\theta + (1-2\sigma)\frac{a}{2}\theta\sin\theta\right]\frac{2\sin\alpha}{\alpha+\sin\alpha\cos\alpha} \tag{IV.78}$$

$$-\frac{2\mu v}{q} = \left[-(1-\sigma)a\ln r\sin\theta + (1-2\sigma)\frac{a}{2}\theta\cos\theta - \frac{a}{2}\sin\theta\right]\frac{2\sin\alpha}{\alpha+\sin\alpha\cos\alpha} \tag{IV.79}$$

Now, although log terms appear in the displacements, there are no singularities. The displacements become large as $r \to \infty$ merely because the wedge is infinite in extent. Further, a force balance again establishes that a reaction force of magnitude $-2\,q\,a\sin\alpha$ is needed, but this time located at $r = \infty$.

In recapitulation, integration along path I or II in the strip $[0, 8]$ represents an inversion to the stress function resulting from a reaction load concentrated at the apex; integration along path III in the strip $[-1, 0]$ represents an inversion to the stress function resulting from a reaction load distributed uniformly over the radial boundary of the wedge along any arc $a < r < \infty$. Finally, it is readily shown that inversion along path IV or any path to the left leads to a tangetial boundary stress other than that specified for this problem. Furthermore, such a path of integration will give rise to stresses, in the region $r > a$, which will go to infinity as $r \to \infty$; physically this can not be accepted.

It remains to investigate what happens if the path of integration is chosen to the right of path I and which is also anywhere to the right of the first conjugate complex pair of roots. Let us first examine the contribution of the first complex pair of roots, i.e. $p = 8.04 \pm i\,4.19$. Consider the region $r < a$. The contribution of this pair of roots to the tangantial stress can be written in the form

$$\sigma_\theta = \left(\frac{r}{a}\right)^{-9.04}\left[F_1(\theta)\cos\left(4.19 \ln\frac{r}{a}\right) + F_2(\theta)\sin\left(4.19 \ln\frac{r}{a}\right)\right] \tag{IV.80}$$

where $F_1(\theta)$ and $F_2(\theta)$ are trigonomatric functions of the angle θ. Integrating (IV.80) from $r = 0$ to $r = a$ will yield the total tangantial load on any radial line from the apex to $r = a$. This total load should be finite, however it can easily be shown by actually carrying out the integral

$$\int_0^a \sigma_\theta \, dr$$

that the result is an infinite force. It can be further shown that the contribution of all the other roots, to the right of the first pair, will lead to the same inconsistency. On this basis we eliminate any such integration path.

G. The Stress Field Around the Crack ($\alpha = \pi$)

As the flank angle increases beyond 180°, the sector defficiency becomes, at first, a wide-angled crack and then it gradually approaches a radial line-crack in the limit $2\alpha = 2\pi$. In this case (IV.28) becomes

$$-\frac{\Phi}{q a^2} = \frac{1}{2\pi i}\int_{c-i\infty}^{c+i\infty} \frac{-(\cos p\theta\cos\theta + p\sin p\theta\sin\theta)}{(p+1)\,p\,(p-1)\cos p\pi}\left(\frac{a}{r}\right)^{p-1} dp \tag{IV.81}$$

The roots of the denominator are all simple and real and occur at -

$$p = -1,\ 0,\ +1,\ (1/2) - m, \text{ where } m = 0, \pm 1, \pm 2, \text{ etc}$$

these poles are illustrated in Figure IV.3.

It can easily be shown that a path of integration in (IV.81) anywhere to the right of p= 3/2 will produce similar inconsistencies to those that were produced, in the case of $2\alpha = 30^{\circ}$, where the path was chosen to the right of the first conjugate pair of poles in the right half of the p - plane. If a path of integration is chosen anywhere to the left of p = -1 then it is not possible to satisfy the prescribed boundary conditions, similar result was found in the case $2\alpha = 30^{\circ}$. Therefore it remains to investigate the five paths of integration which are shown in Figure IV. 3.

Consider first the path I. Using the residue theory the stress function, for r < a, is

$$\frac{\phi}{q_0 a^2} = -\frac{1}{2}\left(\frac{r}{a}\right)^2 + \left(\frac{r}{a}\right)\frac{2\alpha\cos\theta}{2\alpha+\sin 2\alpha} - \frac{1}{2} + \left(\frac{r}{a}\right)^{\frac{3}{2}}\frac{2}{3\pi}\left[3\cos\frac{\theta}{2} + \cos\frac{3}{2}\theta\right] \tag{IV.82}$$

$$+\left(\frac{r}{a}\right)^{\frac{1}{2}}\frac{2}{3\pi}\left[3\cos\frac{\theta}{2}+\cos\frac{3\theta}{2}\right]+\sum_{n=1}^{\infty}\left(\frac{a}{r}\right)^{-n-\frac{3}{2}}\left[\frac{-\left(n+\frac{3}{2}\right)\cos\left(n-\frac{1}{2}\right)+\left(n-\frac{1}{2}\right)\cos\left(n+\frac{3}{2}\right)\theta}{\left(n-\frac{1}{2}\right)\left(n+\frac{1}{2}\right)\left(n+\frac{3}{2}\right)2\pi(-1)^n}\right]$$

The third term on the right hand side of (IV. 82), which is a constant, is generated by the pole at p = 1, obviously then the path of integration can be moved across p = 1 without changing the resultant stress dield. Therefore paths I and II are equivalent. The fifth term in (IV. 82) is generated by the pole at p = 1/2, corresponding to this term the tangential stress component is

$$\sigma_\theta = q_0 a^4\left[\left(\frac{r}{a}\right)^{-\frac{3}{2}}\frac{2}{3\pi}\left(3\cos\frac{\theta}{2}+\cos\frac{3\theta}{2}\right)\right]$$

It can easily be shown that the above component of σ_θ makes the integral

$$\int_0^a \sigma_\theta\, dr$$

become infinite. As described previously, physically such a result is unacceptable. This consideration eliminated path II (and path I).

Consider now path III. The second term in (IV. 82) is generated by the pole at p = 0. Since this term is proportional to r cos θ it can be easily verified that it does not produce any stresses. Therefore paths III and IV are equivalent. The fourth term in (IV. 82) is generated by the pole

at p = - 1/2, it can easily be seen that this term gives rise to stress singularities at r = 0, which are proportional to $r^{1/2}$. However the remaining part of the field is well behaved and physically acceptable. It remains to investigate path V. For this last case the stress function, for the region r > a is

$$\frac{\Phi}{qa^2} = -\left(\frac{r}{a}\right)^{\frac{3}{2}}\frac{2}{3\pi}\left[3\cos\frac{\theta}{2}+\cos\frac{3}{2}\theta\right]-\left(\frac{r}{a}\right)^{\frac{1}{2}}\frac{2}{3\pi}\left[3\cos\frac{\theta}{2}+\cos\frac{3}{2}\theta\right]$$
$$-\sum_{1}^{\infty}\left(\frac{a}{r}\right)^{n-\frac{1}{2}}\left[\frac{-(n+\frac{3}{2})\cos(n-\frac{1}{2})\theta+(n-\frac{1}{2})\cos(n+\frac{3}{2})\theta}{(n-\frac{1}{2})(n+\frac{1}{2})(n+\frac{3}{2})2\pi}\right](-1)^n \qquad \text{(IV.83)}$$

If the stresses are calculated from (IV.83) and then these stresses are used to calculate forces on an arc at r = ∞ , these forces will be infinite. These infinite forces can be traced to the first term in (IV.83), that is to the effect of the pole at p = -1/2. Such large forces for large r are physically unacceptable. On this basis path V cannot be accepted.

On the basis of the foregoing arguments it is deduced that the path of integration can be anywhere between p = -1/2 and p = 1/2. And, such a path of integration will produce a square - root singularity at r = 0.

Finally, the required stress function will have the form (neglecting terms which do not affect the stresses),
for r < a

$$-\frac{\Phi}{qa^2} = \frac{1}{2}\left(\frac{r}{a}\right)^2-\left(\frac{r}{a}\right)^{\frac{3}{2}}\frac{2}{3\pi}\left[3\cos\frac{\theta}{2}+\cos\frac{3}{2}\theta\right]$$
$$-\sum_{n=1}^{\infty}\left(\frac{a}{r}\right)^{n-\frac{3}{2}}\left[\frac{-(n+\frac{3}{2})\cos(n-\frac{1}{2})\theta+(n-\frac{1}{2})\cos(n+\frac{3}{2})\theta}{(n-\frac{1}{2})(n+\frac{1}{2})(n+\frac{3}{2})(-1)^n}\right] \qquad \text{(IV.84)}$$

for r > a

$$-\frac{\Phi}{qa^2} = \left(\frac{r}{a}\right)^{\frac{1}{2}}\frac{2}{3\pi}\left[3\cos\frac{\theta}{2}+\cos\frac{3}{2}\theta\right]$$
$$+\sum_{n=1}^{\infty}\left(\frac{a}{r}\right)^{n-\frac{1}{2}}\left[\frac{-(n+\frac{3}{2})\cos(n-\frac{1}{2})\theta+(n-\frac{1}{2})\cos(n+\frac{3}{2})\theta}{(n-\frac{1}{2})(n+\frac{1}{2})(n+\frac{3}{2})(-1)^n}\right] \qquad \text{(IV.85)}$$

for r $\ll$ a, the stress - displacement field becomes

$$-\frac{\sigma_\theta}{qa^2} = -\frac{2}{\pi}\left(\frac{a}{r}\right)^{\frac{1}{2}}\cos^3\frac{\theta}{2} + 1 \qquad \text{(IV.86 a)}$$

$$-\frac{\sigma_r}{qa^2} = -\frac{2}{\pi}\left(\frac{a}{r}\right)^{\frac{1}{2}}\cos\frac{\theta}{2}\left[1+\sin^2\frac{\theta}{2}\right] + 1 \qquad \text{(IV.86 b)}$$

$$-\frac{\tau_{r\theta}}{q} = -\frac{2}{\pi}\left(\frac{a}{r}\right)^{\frac{1}{2}}\cos^2\frac{\theta}{2}\sin\frac{\theta}{2} \qquad \text{(IV.86 c)}$$

Note that the constant terms in the stress field have been retained in order to guarantee that the tangential stress approaches a non-zero uniform value at the boundary ($\theta = \pm \pi$). The displacement field is given by

$$-\frac{2\mu u}{q} = (1-2\sigma)r - (1-\sigma)\frac{4}{\pi}\sqrt{ar}\left[\cos\frac{\theta}{2} + \sin^2\frac{\theta}{2}\cos\frac{\theta}{2}\right] + \sigma\frac{4}{\pi}\sqrt{ar}\cos^3\frac{\theta}{2} \qquad \text{(IV.87 a)}$$

$$-\frac{2\mu v}{q} = -(1+\sigma)\frac{4}{\pi}\sqrt{ar}\left[\sin\frac{\theta}{2} - \frac{1}{3}\sin^3\frac{\theta}{2}\right] + (2-\sigma)\frac{4}{\pi}\sqrt{ar}\left[\sin\frac{\theta}{2} + \frac{1}{3}\sin^3\frac{\theta}{2}\right] \qquad \text{(IV.87 b)}$$

It is interesting to evaluate the displacements at the boundary, $\theta = \pi$,

$$-\frac{2\mu u}{q} = (1-2\sigma)r - (1-\sigma)\frac{4}{\pi}\sqrt{ar} \qquad \text{(IV.88 a)}$$

$$-\frac{2\mu v}{q} = \frac{8}{\pi}(1-\sigma)\sqrt{ar} \qquad \text{(IV.88 b)}$$

The tangential displacement is negative and increases with r. The radial displacement is positive for small r and then becomes negative.

APPENDIX A

In this Appendix it will be shown that the condition expressed by equation (IV. 8) is satisfied. This condition is necessary for the previous mathematical formulations to hold, and this condition is

$$r^{p}\Phi(r,\theta) = 0 \qquad \text{at} \quad r=0 \qquad \text{and} \quad r=\infty \tag{IV. 1 A}$$

for the case $2\alpha = 30^{\circ}$ there are two solutions, one solution permits a point load at the apex to balance the load on the faces of the wedge, the other solution allows a balancing force at infinity. Let us consider these two solutions, in the above order, separately.

For $r < a$

$$-\frac{\Phi}{q a^2} = \frac{1}{2}\left(\frac{r}{a}\right)^2 - \left(\frac{r}{a}\right)\frac{\sin\alpha\cos\theta + \theta\sin\alpha\sin\theta + \alpha\cos\alpha\cos\theta}{\alpha + \sin\alpha\cos\alpha} + \text{power series of } (r/a) \tag{IV. 2 A}$$

the series contains (r/a) to the power of 9 or greater.

For $r > a$

$$-\frac{\Phi}{q a^2} = \text{power series of } (r/a) \tag{IV. 3 A}$$

the series in (IV. 3 A) contains (r/a) to the power of -7 or less. Remembering that a change of variable $p + 1 = p$ has been made in the complex plane, the path of integration can be expressed by $C = 0 + \delta$ where $0 < \delta < 8$.

Therefore the following has to hold

$$r^{\delta-1}\Phi = 0 \qquad \text{at } r = 0 \quad \text{and } r = \infty$$

from (IV. 2 A) the lowest power of r in $r^{\delta-1}\Phi\ (r, \theta)$ is δ and therefore when $r = 0$, $r^{\delta-1}\Phi\ (r, \theta) = 0$.

From (IV. 3A) the largest power of r in $r^{\delta-1}\Phi\ (r, \theta)$ is $\delta - 8$ and therefore when $r = \infty$, $r^{\delta-1}\Phi\ (r, \theta) = 0$.

Now consider the second solution.

For $r < a$

$$-\frac{\Phi}{q a^2} = \frac{1}{2}\left(\frac{r}{a}\right)^2 + \text{power series of } (r/a) \qquad \text{(IV.4 A)}$$

the series is the same as in (IV.2 A)

For $r > a$

$$-\frac{\Phi}{q a^2} = \left(\frac{r}{a}\right)\frac{\sin\alpha\cos\theta + \theta\sin\alpha\sin\theta + \alpha\cos\alpha\cos\theta}{\alpha + \sin\alpha\cos\alpha} + \text{power series of } (r/a) \qquad \text{(IV.5A)}$$

the series is the same as in (IV.3A).

The path of integration can be defined by $C = -1 + \delta$ where $0 < \delta < 1$. Therefore the following must hold $r^{\delta-2}\Phi(r, \theta) = 0$ at $r = 0$ and $r = \infty$. From (IV.4A) the lowest power or r is δ, therefore when $r = 0$, $r^{\delta-2}(r, \theta) = 0$. From (IV.5A) the largest power of (r) is $\delta - 1$, therefore when $r = \infty$, $r^{\delta-2}\Phi(r, \theta) = 0$.

Consider now the case of the crack, i.e. $\alpha = \pi$. The stress function for this case is given by equations (IV.84) and (IV.85). The path of integration is defined by $C = -1/2 + \delta$, where $0 < \delta < 1$.

From (IV.84) the lowest power of r in $r^{\delta-3/2}\Phi(r, \theta)$ is δ, therefore when $r = 0$ $r^{\delta-3/2}\Phi(r, \theta) = 0$.

From (IV.84 b) the largest power of r in $r^{\delta-3/2}\Phi(r, \theta)$ is $\delta - 1$, therefore when $r = \infty$, $r^{\delta-3/2}\Phi(r, \theta) = 0$

APPENDIX B

In this Appendix the conditions (IV. 14) and (IV. 15) will be verified. Consider first the condition (IV. 15),

$$\lim_{y\to\infty} \bar{\Phi}(x+iy) \longrightarrow 0 \text{ uniformly as } |y| \to \infty \quad . \quad \text{where } p = x + iy$$

By making the substitution $p = x + i\,y$ in equation (IV. 26) and rearranging, the following is obtained

$$\begin{aligned}\frac{\Phi(x+iy)}{-q} = a^{x+1+iy}\Big[&\sin(x+1)\alpha\cosh y\alpha\cos(x-1)\theta\cosh y\theta + \cos(x+1)\alpha\sinh y\alpha\sin(x-1)\theta\sinh y\theta \\ &- \sin(x-1)\alpha\cosh y\alpha\cos(x+1)\theta\cosh y\theta - \cos(x-1)\alpha\cosh y\alpha\sin(x+1)\theta\sinh y\theta \\ &+ i\Big\{-\sin(x+1)\alpha\cosh y\alpha\sin(x-1)\theta\sinh y\theta + \cos(x+1)y\sinh y\alpha\cos(x-1)\theta\cosh y\theta \\ &+ \frac{\sin(x-1)\alpha\cosh y\alpha\sin(x+1)\theta\sinh y\theta - \cos(x-1)\alpha\sinh y\alpha\cos(x+1)\theta\cosh y\theta}{(x^2+x-y^2)(\sin 2x\alpha\cosh 2y\alpha + x\sin 2\alpha) + (2xy+y)(\cos 2x\alpha\sinh 2y\alpha + y\sin 2\alpha)} \\ &+ i\Big\{(2xy+y)(\sin 2x\alpha\cosh 2y\alpha + x\sin 2\alpha) - (x^2+x-y^2)(\cos 2x\alpha\sinh 2y\alpha + y\sin 2\alpha)\Big\}\Big]\end{aligned}$$

(IV. 1B)

It is possible that either $\sin 2x\alpha$ or $\cos 2x\alpha$ will be zero, if either of these conditions exist then the order of magnitude of the terms in the denominator, as $y \to \infty$, can be written

as $$O\{y\sinh 2y\alpha\} + i\{y^2\cosh 2y\alpha\} \qquad \text{(IV. 2B)}$$

or $$O\{y^2\cosh 2y\alpha\} + i\{y\sinh 2y\alpha\} \qquad \text{(IV. 3B)}$$

If $\sin 2x\alpha \neq 0$ and $\cos 2x\alpha \neq 0$ then we have

$$O\left\{y^2 \cosh 2y\alpha\right\} + i\left\{y^2 \cosh 2y\alpha\right\} \qquad \text{(IV. 4 B)}$$

Choosing arbitrarily case (IV. 2B) we can symbolically write

$$\frac{\overline{\Phi}(x+iy)}{-q} = \frac{O\left\{\cosh^2 y\alpha\right\} + i\, O\left\{\cosh^2 y\alpha\right\}}{O\left\{y \sinh 2y\alpha\right\} + i\, O\left\{y^2 \cosh 2y\alpha\right\}} \qquad \text{(IV. 5B)}$$

when $y \to \infty$

Since $\sin h\, 2y\alpha = 2 \sin h\, y\alpha \cosh y\alpha$ therefore as $y \to \infty$ expression (IV. 5 B) tends to zero. It can easily be seen that the cases (IV. 3 B), (IV. 4B) yield the same result.

It follows then that for any finite x, the condition (IV. 15) is satisfied. Consider now the condition (IV. 14),

$$\int_{-\infty}^{\infty} \left|\overline{\Phi}(x+iy)\right| dy \qquad \text{converges as } |y| \to \infty$$

from equation (IV. 1B) we can write

$$\frac{\Phi(x+iy)}{-q} = a^{x+1}\frac{M+iN}{X+iY} \qquad \text{(IV. 6 B)}$$

where

$$M = \cos(y \ln a)\Big[\sin(x+1)\alpha \cosh y\alpha \cos(x-1)\theta \cosh y\theta + \cos(x+1)\alpha \sinh y\alpha \sin(x-1)\theta \sinh y\theta$$
$$- \sin(x-1)\alpha \cosh y\alpha \cos(x+1)\theta \cosh y\theta - \cos(x-1)\alpha \sinh y\alpha \sin(x+1)\theta \sinh y\theta\Big]$$
$$- \sin(y \ln a)\Big[-\sin(x+1)\alpha \cosh y\alpha \sin(x-1)\theta \sinh y\theta + \cos(x+1)\alpha \sinh y\alpha \cos(x-1)\theta \cosh y\theta$$
$$+ \sin(x-1)\alpha \cosh y\alpha \sin(x+1)\theta \sinh y\theta - \cos(x-1)\alpha \sinh y\alpha \cos(x-1)\theta \cosh y\theta\Big]$$

$$N = \sin(y\ln a)\Big[\sin(x+1)\alpha\cosh y\alpha\cos(x-1)\theta\cosh y\theta + \cos(x+1)\alpha\sinh y\alpha\sin(x-1)\theta\sinh y\theta$$

$$- \sin(x-1)\alpha\cosh y\alpha\cos(x+1)\theta\cosh y\theta - \cos(x-1)\alpha\sinh y\alpha\sin(x+1)\theta\sinh y\theta$$

$$+ \cos(y\ln a)\Big[-\sin(x+1)\alpha\cosh y\alpha\sin(x-1)\theta\sinh y\theta + \cos(x+1)\alpha\sinh y\alpha\cos(x-1)\theta\cosh y\theta$$

$$+ \sin(x-1)\alpha\cosh y\alpha\sin(x+1)\theta\sinh y\theta - \cos(x-1)\alpha\sinh y\alpha\cos(x-1)\theta\cosh y\theta\Big]$$

$$X = (x^2 + x - y^2)(\sin 2x\alpha\cosh 2y\alpha + x\sin 2\alpha) + (2xy+y)(\cos 2x\alpha\sinh 2y\alpha + y\sin 2\alpha)$$

$$Y = (2xy+y)(\sin 2x\alpha\cosh 2y\alpha + x\sin 2\alpha) + (x^2+x-y^2)(\sin 2x\alpha\cosh 2y\alpha + x\sin 2\alpha)$$

from (IV. 6 B)

$$\frac{\overline{\Phi}(x+iy)}{-q} = a^{x+1}\,\frac{(MX+NY)+i(NX-MY)}{X^2+Y^2}$$

$$= a^{x+1}\,\frac{P+iQ}{X^2+Y^2}$$

where

$$P = MX + NY$$
$$Q = NX - MY \qquad \text{(IV. 7B)}$$

therefore

$$\left|\frac{\overline{\Phi}(x+iy)}{q\,a^{x+1}}\right| = \frac{\sqrt{P^2+Q^2}}{X^2+Y^2} \leq \frac{|P|+|R|}{X^2+Y^2} \qquad \text{(IV.8B)}$$

since

$$P^2+Q^2 < (|P|+|Q|)^2$$

But

$$|P| \leq |M||X| + |N||Y|$$

$$|Q| \leq |N||X| + |M||Y|$$

and

$$|M| \leq 2\cosh^2 y\alpha \quad , \qquad |N| \leq 2\cosh^2 y\alpha$$

therefore

$$\left|\frac{\overline{\Phi}(x+iy)}{q\,a^{x+1}}\right| \leq 2\cosh^2 y\alpha \;\; \frac{|X|+|Y|}{X^2+Y^2} \qquad \text{(IV.9B)}$$

From (IV.9 B)

$$\int_{-\infty}^{\infty} |\Phi|\,dy < \int_{-\infty}^{\infty} 2q\,a^{x+1}\cosh^2 y\alpha \;\frac{|X|+|Y|}{X^2+Y^2}\,dy \qquad \text{(IV.10B)}$$

for a large y we again have the three possible conditions (IV.2 B), (IV.3 B), (IV.4 B). It is sufficient to consider only one of these.

Take arbitrarily

$$|X| \leq |y||\sinh 2y\alpha|$$

$$|Y| \leq |y^2||\cosh 2y\alpha|$$

it follows

$$\frac{|X|+|Y|}{X^2+Y^2} < \frac{2y^2\cosh 2y\alpha}{y^4\cosh^2 2y\alpha} = \frac{2}{y^2\cosh 2y\alpha} \qquad \text{(IV.11 B)}$$

assume that "d" is some large, but finite, value of y for which (IV. 11 B) holds. Therefore the integral (IV. 10 B) can be written

$$\int_{-\infty}^{\infty} |\overline{\Phi}| dy < 2\int_{0}^{d} 2q\, a^{x+1} \cosh^2 y\alpha \frac{|X|+|Y|}{X^2+Y^2} dy + \int_{d}^{\infty} 2q\, a^{x+1} \frac{dy}{y^2} \qquad \text{(IV. 12 B)}$$

The second integral on the right hand side is finite, it remains to prove that the first integral is also finite. Since the first integral is over a finite range the only way that it can become infinite is if the intergrand has poles. The only way that the poles can exist if $X^2 + Y^2 = 0$ or $X + i\,Y = 0$, however this is the same equation which defines the poles of $\Phi(p)$. Therefore it the line of integration in the first integral of (IV. 12 B) is taken between the poles, as it has to be, then this integral will be finite. This proves that

$$\int_{-\infty}^{\infty} \left|\overline{\Phi}(x + i\,y)\right| dy \text{ converges.}$$

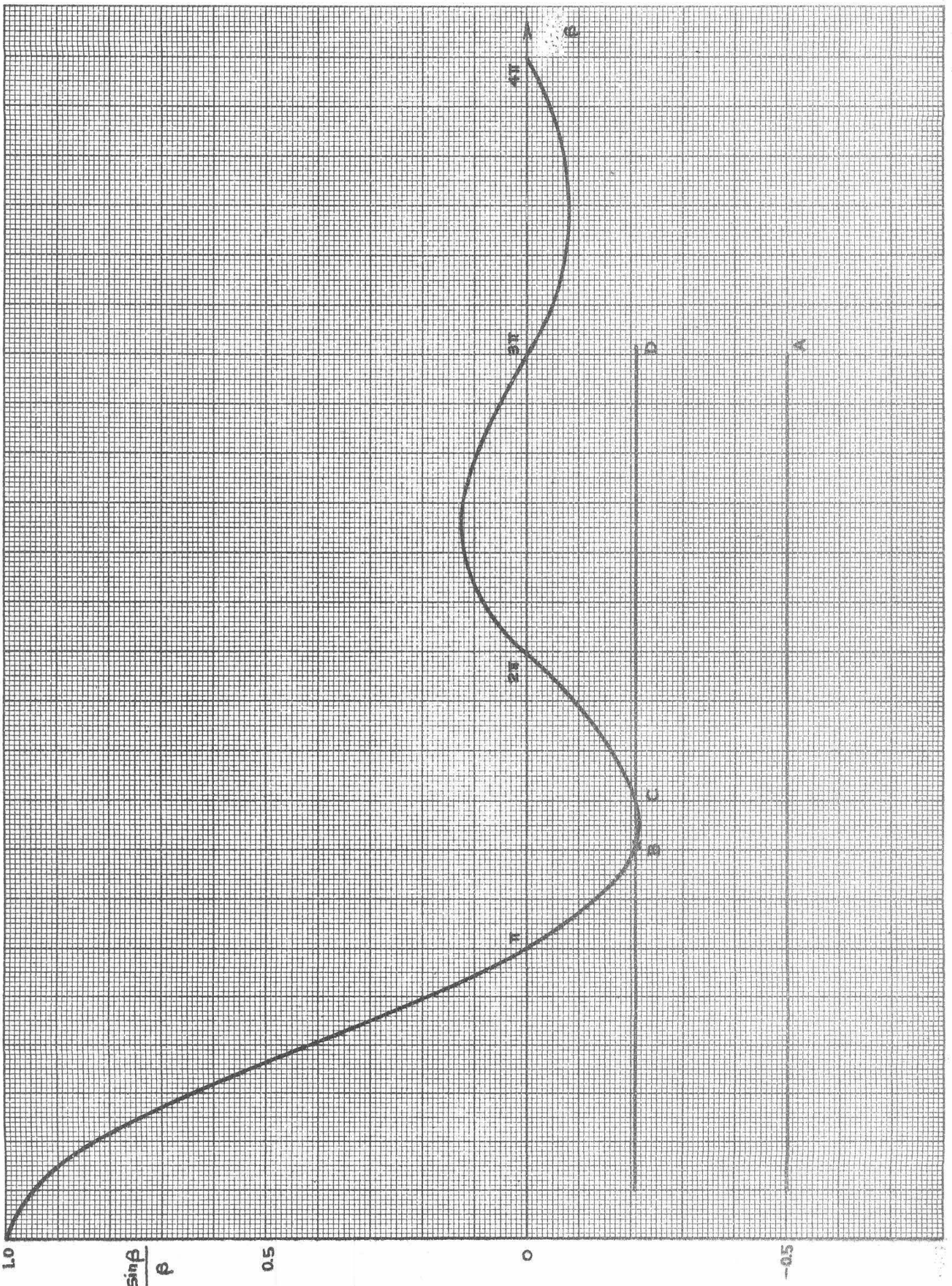

FIG. IV. 1

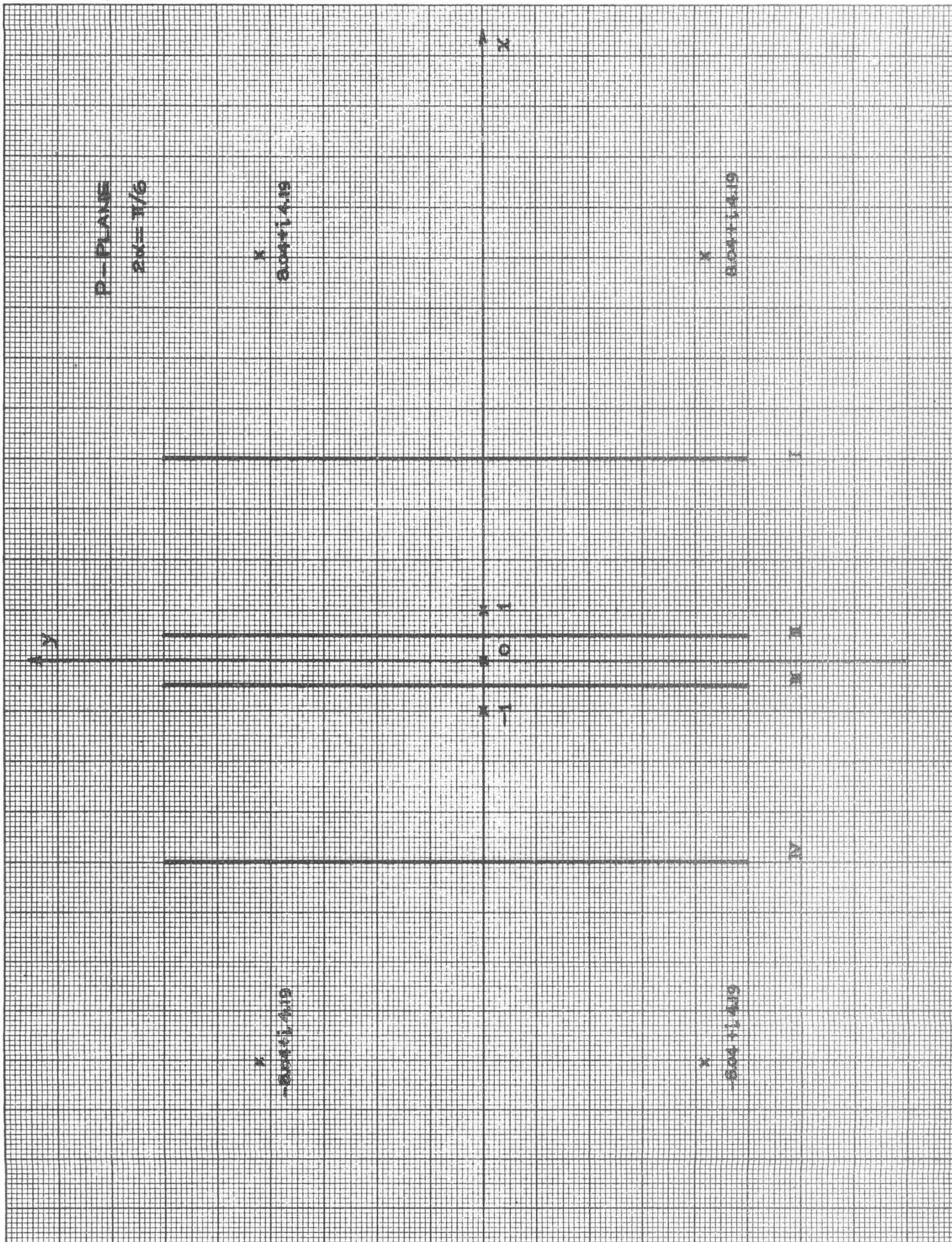
P—PLANE
2α= π/6
x
y
8.04+i 4.19
8.04+i 4.19
-8.04+i 4.19
-8.04+i 4.19
1
0
-1
I
II
III
IV

FIG. IV. 2

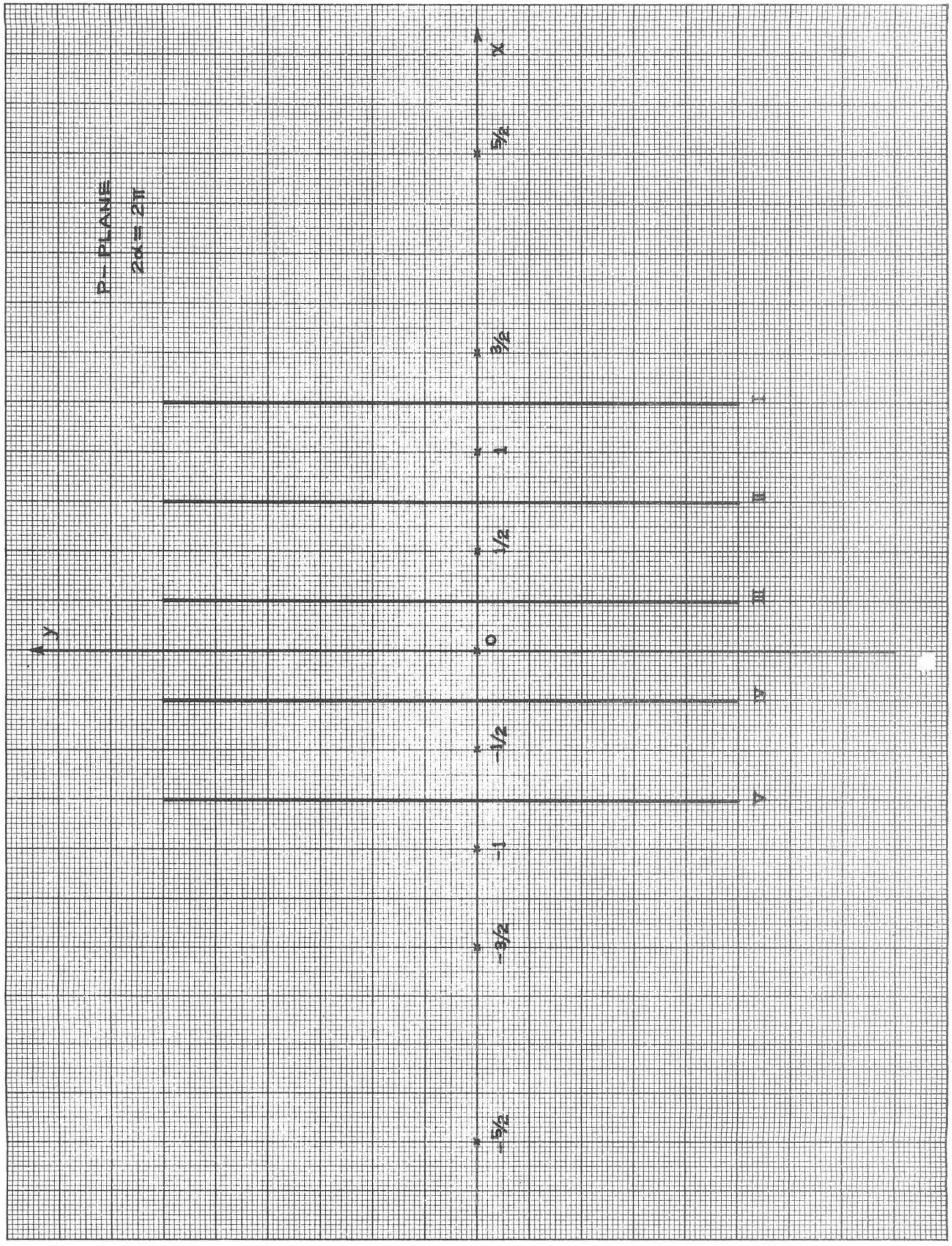

FIG. IV. 3